The GTPase-activating protein RN-tre controls focal adhesion turnover and cell migration.

RN-tre controls focal adhesion turnover and cell migration

Andrea Palamidessi[1*], Emanuela Frittoli[1*], Nadia Ducano[2*], Nina Offenhauser[1], Sara Sigismund[1], Hiroaki Kajiho[1], Dario Parazzoli[1], Amanda Oldani[1], Marco Gobbi[3], Guido Serini[2], Pier Paolo Di Fiore[1,4,5], Giorgio Scita[1,5] and Letizia Lanzetti[2]

[1]IFOM, Fondazione Istituto FIRC di Oncologia Molecolare, Via Adamello 16, 20139 Milano, Italy;
[2]Dipartimento di Scienze Oncologiche, Università degli Studi di Torino, Istituto per la Ricerca e la Cura del Cancro, Str. Provinciale 142 10060 Candiolo, Torino, Italy;
[3]Dipartimento di Biochimica e Farmacologia Molecolare, "Mario Negri" Istituto per la Ricerca Farmacologica, 20156 Milano, Italy
[4]Dipartimento di Oncologia Sperimentale, Istituto Europeo di Oncologia, 20141 Milano, Italy;
[5]Dipartimento di Medicina, Chirurgia ed Odontoiatria, Universita' degli Studi di Milano, 20122 Milan, Italy.

[*]These authors equally contributed to the work

Correspondence should be addressed to:
Giorgio Scita
IFOM, Fondazione Istituto FIRC di Oncologia Molecolare
Via Adamello 16, 20139 Milan, Italy;
e-mail: giorgio.scita@ifom-ieo-campus.it

Letizia Lanzetti
Istituto per la Ricerca e la Cura del Cancro
Str. Provinciale 142, 10060 Candiolo, Turin Italy
Tel. +39 0119933508 Fax +39 0119933524
e-mail: letizia.lanzetti@ircc.it

Running title: RN-tre regulates cell migration

ABSTRACT

Background: Integrin-mediated adhesion of cells to the extracellular matrix (ECM) relies on the dynamic formation of focal adhesions (FA), which are biochemical and mechanosensitive platforms composed of a large variety of cytosolic and transmembrane proteins. During migration, there is a constant turnover of ECM contacts that initially form as nascent adhesions at the leading edge, mature into FA as actomyosin tension builds up, and are then disassembled at the cell rear, thus allowing for cell detachment. While the mechanisms of FA assembly have largely been defined, the molecular circuitry that regulates their disassembly still remains elusive.

Results: Here, we show that RN-tre, a GTPase-activating protein (GAP) for Rabs, including Rab5 and Rab43, is a novel regulator of FA dynamics. We found that RN-tre localises to FA and its genetic deletion leads to increased rates of β1-integrin endocytosis, enhanced FA turnover and persistent directed cell migration. Importantly, all these effects are mediated by the GAP activity of RN-tre and rely on Rab5.

Conclusions: Our findings reveal that RN-tre, by targeting endocytic trafficking of β1-integrin and FA dynamics, is a novel regulator of growth-factor-directed cell migration.

HIGHLIGHTS

- RN-tre localises to focal adhesions
- Genetic deletion of RN-tre increases active-Rab5 in response to growth factors
- RN-tre controls β1-integrin endocytosis and focal adhesion turnover
- By negatively regulating Rab5 function, RN-tre restricts directed cell migration

INTRODUCTION

Engagement of integrin transmembrane receptors with extracellular matrix (ECM) ligands is a central step in the formation of FA. These structures are highly dynamic, undergoing a spatio-temporally regulated turnover, particularly during cell migration. Under these conditions, FA form at the leading edge as nascent adhesions that mature into large FA through the sequential recruitment of a wide number of components, establishing stable attachment of cells to the substrate. FA must, then, disassemble to allow cell rear detachment and effective locomotion [1-3]. In the past two decades, many molecular details of FA assembly have been identified. Much less is known, however, about the mechanisms and signalling pathways that control FA turnover. A process that is emerging as essential for the latter regulatory step is membrane trafficking [4]. FA disassembly, for example, has been shown to occur through a targeted mechanism involving MTs, dynamin, clathrin, and specific clathrin adaptors that locally promote integrin endocytosis [5-9]. Integrin trafficking in the endosomal compartment is controlled by small GTPases of the Rab5-subfamily: Rab5 and Rab21, with the latter playing a crucial role both in integrin endocytosis and recycling [5, 10]. Rab5, is a master regulator of early endosomes [11], where integrins invariably accumulate for subsequent sorting [4]. Recently, Rab5 has also been found to control integrin turnover within long-lived ECM adhesions required for the maintenance of tissue architecture, such as the myotendineous junctions of Drosophila embryos [12]. Notably, Rab5 participates to cell migration, not only by regulating integrin trafficking [5], but also by promoting endo/exocytic cycles of the small GTPase Rac that is required for spatial resolution of Rac-dependent motogenic signals and the formation of migratory protrusions ([13, 14] and reviewed in [15]). Thus, Rab5 is emerging as a central trafficking molecule that directly influences several aspects of cell migration. How the activity of this small GTPase is regulated during FA turnover is, however, not known.

Like all small GTPases, Rab5 activity is controlled by guanine nucleotide exchange factors, RabGDI, and GTPase activating proteins (GAP) [16, 17]. Among the latter proteins, RN-tre, also named USP6NL, has been shown to enhance GTP hydrolysis of Rab5 [18, 19] and more recently also of Rab43, a GTPase involved in retrograde transport pathways [20-23]. Consistent with its biochemical activity on Rab5, RN-tre expression is sufficient to inhibit Rab5-dependent transferrin and EGF internalisation [18]. This endocytic role is evolutionary conserved from Drosophila cells, where RN-tre was identified in a genomic screen for regulators of endocytosis [24], to Zebrafish embryos, where RN-tre was shown to inhibit Rab5-dependent endocytosis of Fgf8 [25]. RN-tre also participates in Rab5-dependent signalling to actin dynamics. The ectopic expression of RN-tre, but not its GAP-defective mutant, impairs Platelet Derived Growth Factor (PDGF)-mediated formation of a set of specialised migratory and endocytic actin-based protrusion [19], commonly referred to as circular dorsal ruffles [26].

Two recent and independent proteomic studies identified RN-tre among the components of FA [27, 28], but its function in the formation or dynamic remodelling of these structures has never been addressed. Here, we set out to investigate this issue further by exploring the role of RN-tre in FA turnover and cell migration.

RESULTS

RN-tre localises to FA

RN-tre displays a complex pattern of intracellular localisation, but is predominantly enriched at the plasma membrane (PM) [19, 29]. We used Total Internal Reflection Fluorescence (TIRF) microscopy in living immortalised mouse embryo fibroblasts (MEF) expressing GFP-tagged RN-tre to investigate its PM localisation in more details. We observed that GFP-RN-tre accumulated in FA where it co-localised with two major components of the integrin adhesome, namely vinculin and paxillin (Fig. 1A). This localisation was confirmed by confocal analysis on fixed cells expressing RN-tre fused to GFP or HA tags (Fig. S1A, B). In addition, RN-tre extensively co-localised in adhesive sites with the ECM-bound/active conformation of β1-integrin, as recognised by the conformation-specific 9EG7 antibody [30] (Fig. 1B). Co-localisation between RN-tre and active-β1-integrin was also evident in fibrillar adhesions which are structures that arise from the sliding of tensin-bound active α5β1-integrin along actin stress fibres (Fig. 1B) [31, 32]. Thus, RN-tre is a newly identified component of adhesive sites. Notably, another known GAP for Rab5, RabGAP-5 [20] displayed a diffuse cytoplasmic distribution, as previously shown [21]. Contrary to GFP-RN-tre, GFP-RabGAP-5 did not accumulate in FA (Fig. S1C), suggesting that RN-tre might control the function of Rab5 in cell adhesion and migration.

RN-tre is a GAP for Rab5 *in vitro* and *in vivo*

The GAP activity of RN-tre has multiple targets *in vitro* [20]. In living cells, it has been reported to negatively regulate cell processes that are under the control of Rab5 [18, 19] and Rab43 [21]. The observation that RN-tre is in FA, together with evidence showing that Rab5 participates in integrin internalisation [5], prompted us to re-evaluate the effects of RN-tre in stimulating GTP hydrolysis focusing primarily on Rab5 both *in vitro* and *in vivo*.

To this end, we compared the catalytic activity of RN-tre with that of RabGAP-5 using Rab5 as a substrate. We first tested the activity of the isolated catalytic TBC domains (aa 2-395 for both RN-tre and RabGAP-5), in order to avoid the potential influence of other regions of the proteins, whose regulatory activity *in vivo* could have not been reproduced in the *in vitro* assay. Next, we also verified the catalytic activity of full-length RN-tre and RabGAP-5 (see below). To compare the efficiency of the TBC domains of RN-tre and RabGAP-5 in accelerating the intrinsic rate of GTP hydrolysis of Rab5, we employed an enzymatic assay that measures the amounts of phosphate released [33] over time by purified GTP-loaded Rab5 in the presence of increasing catalytic concentrations of either RN-tre or RabGAP-5 TBC domains (purified proteins employed in the assays are shown in Fig. S2B). Notably, neither the various GAP preparations nor the buffers used contained detectable traces of inorganic phosphate (Fig. S2A). Furthermore, a mutant of the TBC domain of RN-tre in the catalytic arginine was completely inactive (Fig. S2A). The intrinsic rate of GTP hydrolysis by Rab5 was 8.4 X 10^{-4} s^{-1} at 25^{o}C remarkably similar to previously reported measurements [18, 34, 35] (Fig. 2A rate of Rab5 hydrolysis measured in absence of TBC domains). More importantly, both the TBC domains of RN-tre (RN-tre-TBC) and RabGAP-5 (RabGAP-5-TBC) accelerated the rate of hydrolysis with similar catalytic efficiency with values of Kcat/Km in the range of those reported for a variety of other TBC/GAP domains for different Rab proteins [33] (Fig. 2A and C). We further verified the GAP activity of the TBC domains of RN-tre and RabGAP-5 using two independent GAP assays with radiolabelled GTP: a filter binding and a Thin-Layer Chromatography assays. The latter assay enables the separation of GTP and GDP and thus the direct measurement of the amounts of GTP-to-GDP hydrolysis of Rab5 in the presence or absence of the GAP domains. Both TBC domains display similar and readily detectable GAP activities (Fig S2B, C). Thus, under our experimental conditions, the catalytic efficiency of RN-tre-TBC was nearly identical to that of RabGAP-5-TBC. We

performed the same set of experiments using full length RN-tre and RabGAP-5, which were both purified to homogeneity from insect cells (see Fig. S2D). Full-length proteins were more efficient in accelerating the rate of hydrolysis of GTP-loaded Rab5 as compared to their respective, isolated, TBC domains. Importantly, they display similar catalytic efficiency, being full length RN-tre a slightly more efficient catalyst than RabGAP-5 (Fig. 2B and C). We thus concluded that RN-tre and RabGAP-5 are *bona fide* GAP for Rab5 displaying similar catalytic efficiency, at least, *in vitro*.

Next, we tested RN-tre GAP activity on Rab5 *in vivo*. To this end, we generated mice with a targeted deletion of the *RN-tre* locus (the knockout strategy and the detailed description of mice generation are described in Fig. S2E-L). Mice bearing homozygous *RN-tre* deletion were viable and fertile and did not display gross abnormalities. We evaluated the GTP-bound state of Rab5 in fibroblasts established from *RN-tre* -/- (KO) and *RN-tre* +/+ (WT) embryos at 13.5 days post-coitum. The amount of Rab5-GTP was measured taking advantage of the Rab5-binding domain (RBD) of the early–endosomal autoantigen 1 (EEA1) which is a Rab5-effector that binds to active-Rab5 on endosomes [36, 37]. Two regions in EEA1 are implicated in this binding. One is located in the N-terminus of the protein, while the other one encompasses amino acids 1257-1411 in the C-terminal portion and shares homology with the RBD domain of Rabaptin-5 [36]. This latter region, fused to Glutathione-S- Transferase (GST), was purified and its ability to interact specifically with the active form of Rab5 was confirmed by using lysates of 293T cells transfected with dominant-active (Rab5Q79L) or dominant-negative (Rab5S34N) Rab5 mutants (Fig. 2D). Activation of Rab5 is elicited by Epidermal Growth Factor (EGF) stimulation [38]. Similarly, we found that also PDGF treatment stimulates Rab5 activation in a time dependent fashion (with a peak of activation ~ 7 min following PDGF stimulation) in *RN-tre* KO primary embryonic fibroblasts (PEF) (Fig. 2E). We then compared the levels of Rab5-GTP in PDGF-stimulated WT or KO

PEF. Since the levels of endogenous active-Rab5 were undetectable in WT fibroblasts, we ectopically transfected small amounts of Rab5 into both WT and KO cells. Genetic removal of RN-tre led to a significant increase in the amount of PDGF-induced, GTP-loaded Rab5 (Fig. 2F), without altering the levels of expression of the Rab5 effectors, Rabaptin-5 and EEA1 (not shown). We extended and validated this finding in immortalised *RN-tre* KO MEF, stably expressing either an inducible empty vector (KO) or wild type RN-tre (KO+RN-tre) or the RN-tre GAP-defective mutant RN-tre^{R150A} [18] (KO+RN-treR150A) (Fig. S2M and Fig. 2G). Re-expression of wild type RN-tre, but not of RN-tre^{R150A} or the empty vector, impaired PDGF-induced Rab5 activation, indicating that RN-tre is a GAP for Rab5 *in vivo* (Fig. 2G).

RN-tre displays GAP activity also toward Rab43 [20], the GTP-bound form of which may, therefore, be elevated in *RN-tre* KO MEF. This, in turn, could stimulate PDGF-dependent loading of GTP on Rab5 via unknown mechanisms. In addition to be a GAP for Rab5 and Rab43, RN-tre binds, at least in yeast two-hybrid, to Rab30 [20]. We, therefore, analysed also Rab30. Expression of a dominant negative Rab43 or Rab30 in *RN-tre* KO MEF had no effects on Rab5-GTP levels (Fig. S2N, O), suggesting that these GTPases unlikely influence PDGF-induced Rab5 activation.

We also looked at the localisation of endogenous Rab5 in our fibroblasts. The size of Rab5-endosomes appeared to be generally increased in the KO compared to WT fibroblasts (Fig. S2P). This was particularly evident in 30% of the cells (Fig. S2P). These results are compatible with the higher activity of Rab5 in the *RN-tre* KO cells.

Having previously shown that RN-tre inhibits receptors endocytosis [18], we analysed the kinetic of endocytosis of the transferrin receptor or of the EGFR (elicited by stimulation with low or high doses of EGF) in *RN-tre* WT and KO MEF. As expected for cells in which Rab5 is more active, endocytosis of both receptors was slightly, but reproducibly, higher in *RN-tre*-null cells (Fig. S3A, B).

In conclusion, the sum of these data demonstrates that genetic removal of RN-tre increases Rab5 activation and Rab5-dependent endocytic processes *in vivo*.

RN-tre and Rab5 regulate β1-integrin endocytosis and FA turnover

Rab5 activity promotes β1-integrin endocytosis and cell adhesion to ECM proteins [5] but how its function is down-modulated in adhesion/migration settings is currently unknown. Our results showing that *RN-tre* KO fibroblasts have higher levels of active-Rab5, prompted us to investigate the impact of RN-tre on β1-integrin endocytosis in the *RN-tre* KO MEF.

At the cell surface, integrins are present either in ECM-bound/active or ligand-free/inactive conformation [39]. RN-tre genetic deletion did not significantly alter cell surface levels of either total (i.e. inactive plus active) or active β1-integrin measured by ELISA-based detection after surface biotynilation at 4°C as in [40], under conditions of endocytosis blockade (Fig. 3A). Conversely, the internalisation rates of both total and active β1-integrin were increased in the *RN-tre* KO MEF compared to WT cells (Fig. 3B). Importantly, re-expression of RN-tre in KO MEF strongly reduced the rate of β1-integrin endocytosis while the GAP-defective mutant did not (Fig. S3C, D), indicating that, as previously shown for other receptors ([18] and Fig. S3A, B), the GAP activity of RN-tre is essential to regulate β1-integrin internalisation.

We next employed live TIRF microscopy to directly monitor the localisation of Rab5 and RN-tre in motile fibroblasts. To this end GFP-RN-tre, RFP-Rab5A and CFP-paxillin were co-transfected in *RN-tre* KO MEF plated on fibronectin (1 μg/ml) and recorded for 2-4 hours after plating, when adhesions are highly dynamic. Rab5 was primarily present, as expected, into vesicles, while RN-tre was both in adhesive sites and on vesicles. We detected a striking co-localisation of RN-tre and Rab5 on a subset of vesicles that were mainly

associated with FA undergoing rapid remodelling, in particular at the cell rear (Fig. 3C and Movie S1).

Integrin endocytosis is a mechanism to control focal adhesion disassembly [6, 8, 9]. Of note, Rab5 participates to β1-integrin trafficking [5] and, in Drosophila myotendineous junctions, to the turnover of integrin-associated proteins [12]. Having found that RN-tre is in FA and that its GAP function regulates β1-integrin endocytosis, we hypothesised that RN-tre and Rab5 affect FA turnover. To test this possibility, we transfected WT and KO MEF with GFP-paxillin to monitor adhesion dynamics by Fluorescence Recovery After Photobleaching (FRAP) analysis. We analysed FA located at the cell periphery or at the cell rear, and also fibrillar adhesions (Fig. 4A-C). Typically, two to four GFP-paxillin positive FA were analysed per cell. The mean half-time of fluorescence recovery (FRAP t1/2) in the bleached area was determined as an estimate of the stability of adhesion binding (as described in [41]). KO MEF exhibited a significantly faster recovery of GFP-paxillin compared to WT both in peripheral FA (mean FRAP t1/2 of KO = 18.3 ± 1.6 sec. versus FRAP t1/2 of WT = 32.6 ± 2.2 sec.) (Fig. 4A and Movie S2), and in FA at the cell rear (mean FRAP t1/2 of KO = 15.6 ± 1.2 sec. versus FRAP t1/2 of WT = 27.5 ± 2.3 sec.) (Fig. 4B and Movie S3). No significant differences were scored in the turnover of fibrillar adhesions (Fig. 4C and Movie S4). Re-expression of RN-tre, but not of RN-tre^{R150A}, severely affected GFP-paxillin turnover in peripheral FA (mean FRAP t1/2 of KO = 18.7 ± 2.8 sec. versus FRAP t1/2 of KO+RN-tre = 44.5 ± 3.7 sec., FRAP t1/2 KO+RN-treR150A = 17.5 ± 3 sec.) (Fig. 4D and Movie S5). These results strengthen our findings that removal of RN-tre increases β1-integrin endocytosis, in a GAP-dependent manner, further predicting that faster fluorescence recovery of GFP-paxillin might depend on higher levels of active-Rab5 in the KO MEF. To verify this prediction, we silenced all the three isoforms of Rab5 (Rab5A/B/C), which act redundantly in endocytosis [42], or Rab43 in KO MEF transfected with GFP-paxillin. Peripheral GFP-

paxillin-positive FA were subjected to FRAP analysis. Silencing of Rab43 left unperturbed the FRAP t1/2 of KO MEF (19.3 ± 1 sec. in Rab43 knocked down versus 15.4 ± 1.2 sec. in KO MEF silenced with control oligos) (Fig. 4E and Movie S6). Instead, interference with Rab5 isoforms significantly delayed GFP-paxillin turnover (FRAP t1/2 = 34.2 ± 2.1 sec.) (Fig. 4E and Movie S6). Thus Rab5 is required for optimal FA turnover, while the GAP activity of RN-tre negatively regulates it.

Genetic deletion of RN-tre enhances cell migration

Flux of integrins through the endocytic pathway and FA turnover dictate the speed of cell migration ([43] and reviewed in [44]); we thus investigated the effects of RN-tre removal on cell migration on ECM substrates.

We initially tested random cell motility in primary fibroblasts from WT and KO littermate embryos, using Dunn chamber assays, in the absence of any diffusible gradient (Fig. 5A and Movie S7). Under these conditions, both the total distance and cell velocity were increased in fibroblasts lacking RN-tre as compared to WT cells, while directionality, which measures the ability of a cell to move persistently along its migratory path, was not significantly altered (Fig. 5A and Movie S7). These results suggest that RN-tre removal fosters the speed of cell migration, consistent with its role in regulating FA turnover. Next, we used the same Dunn chamber setting, but adding PDGF to one of the well to generate a diffusible gradient, and investigated chemotactic migration of RN-tre or RN-tre^{R150A} –expressing, or control KO MEF. PDGF is a potent motogenic factor for fibroblasts that also induces Rab5 activation in RN-tre-dependent manner (Fig. 2E-G). As expected, genetic deletion of RN-tre increased both the distance and the velocity without affecting the persistency of random cell migration (Fig. 5B and Movie S8). Instead, re-expression of RN-tre, but not of the GAP-defective mutant, had a dramatic inhibitory effect on the ability of cells to move toward the PDGF

gradient, as witnessed by the ~10 fold reduction in forward migration index (Fig. 5B and Movie S8). Notably, and consistently with the effect on β1-integrin endocytosis, RN-tre removal significantly improved the forward migration of cells plated on fibronectin, a ligand for α5β1-integrin, but not on vitronectin, a ligand for αvβ3-integrin (Fig. S5A, B and Movies S9 and S10). Finally, the ectopic expression of RN-tre in HeLa cell impaired EGF-directed cell migration, suggesting that RN-tre is generally implicated in growth factor-mediated motility (Fig. S5C and Movie S11).

Since RN-tre removal enhances the levels of active-Rab5 in response to PDGF stimulation, we next directly investigated whether this small GTPase, rather than other RN-tre targets, was responsible for the altered chemotactic cell migration of *RN-tre* KO MEF. To this end, we silenced all Rab5 isoforms simultaneously, or Rab43 and, as a further control, also Rab30 (Fig. 5C, Movie S12 and Fig. S4). Silencing of Rab5 isoforms severely impaired distance, velocity and forward migration index of *RN-tre* KO MEF (Fig. 5C and Movie S12) as well as of reconstituted cells (not shown). Conversely, silencing of Rab43 or Rab30 had no appreciable effects on any of the migratory parameters measured (Fig. 5C and Movie S12). Thus, collectively, our findings indicate that RN-tre is an essential regulator of chemotactic cell migration by specifically targeting Rab5-mediated β1-integrin endocytosis and FA dynamics.

DISCUSSION

Spatio-temporal control of FA turnover is essential to support cell migration [1, 2, 3]. Our study uncovers RN-tre as a novel and physiologically relevant component of FA that participates to their turnover by controlling Rab5-dependent dynamic association of key FA adaptors like paxillin, and the endocytosis of essential FA components, such as β1-integrin, ultimately impacting on cell migration.

We found that, in accordance with the ability of RN-tre to stimulate GTP hydrolysis on Rab5 ([18] and this study), genetic removal of RN-tre increases the levels of active-Rab5 in fibroblasts fostering cellular processes that depend on Rab5 activation, such as β1-integrin endocytosis. In agreement with endocytosis of integrins as a mechanism to control FA disassembly and cell motility [4, 44, 45], *RN-tre* KO fibroblasts display faster FA turnover and increased cell migration. It is of note that the forward migration index, a parameter that expresses the ability of cells to migrate along with a chemotactic gradient, is improved in *RN-tre* KO fibroblasts, indicating that RN-tre is a relevant player in chemotactic, directional cell migration. This is also supported by recent findings showing that RN-tre participates to the directional migration of border cells in *Drosophila melanogaster* [46], a migratory process in which Rab5 is pivotal [47].

RN-tre is also a GAP for Rab43 [20, 22]. However, the regulation of Rab43 by RN-tre does not seem to be essential for cell migration because silencing of Rab43 does not affect FA turnover or the migratory capabilities of the *RN-tre* KO fibroblasts. Conversely, silencing of Rab5 abrogates all these effects, indicating that they rely on Rab5. Despite these findings, we do not exclude that RN-tre might act in cell migration by also regulating other Rabs in addition to Rab5.

Rab5, like other small GTPases, displays multiple GEFs and GAPs [16, 17]. Intriguingly, in adhesive sites, the recruitment of both its GEF RIN2 [48] and of the GAP RN-tre suggests the

existence of a molecular circuitry that controls the activity of Rab5 specifically during cell adhesion. This appealing hypothesis is supported by the findings showing that RN-tre localises to Rab5-positive vesicles closely associated with active remodelling FA, where RN-tre also accumulates. This localisation is not shared by other GAPs for Rab5, pointing to a possible specific function for RN-tre in this process. Furthermore, this might also reflect a more specific effect of RN-tre in regulating the function of Rab5 on integrin trafficking rather than on other receptors.

In conclusion, we propose that RN-tre acts as a "brake" in cell migration: by turning off Rab5, it inhibits β1-integrin endocytosis and favours FA stability, shifting the balance between adhesion and migration towards a less motile phenotype.

EXPERIMENTAL PROCEDURES

Generation of RN-tre null mice

We generated RN-tre knockout mice by targeting exon 7 and exon 8 of the *RN-tre* gene that encode for a portion of the TBC domain, including Arg150, which is essential for the catalytic activity of RN-tre [18]. A schematic representation of the strategy is presented in Fig. S2E-L. Immortalised fibroblasts from *RN-tre* +/+ (WT) or -/- (KO) embryos were established as described [49].

Cell culture and siRNA

Primary and immortalised embryo fibroblasts were grown in DMEM medium (Lonza) supplemented with 10% South American serum (EuroClone) and 1% L-Glutamine (EuroClone). Transfections were performed using Lipofectamine Plus (Invitrogen), according to the manufacturer's instructions. Serum-starved MEF were stimulated with 10 ng/ml of PDGF (R&D). KO MEF were reconstituted with RN-tre or RN-tre^{R150A} using Tetracycline-inducible lentiviral vectors and grown in DMEM supplemented with 10% Tet system-approved FBS (Clontech). Expression of the RN-tre or RN-tre^{R150A} was achieved by adding doxycycline (0.5 μg/ml, Sigma-Aldrich) 48 h before harvesting cells.

Imaging techniques and quantifications

Immunofluorescence was as in [50]. Primary antibodies were revealed by Alexa Fluor 555-, 488- (Molecular Probes) conjugated secondary antibodies. Confocal analysis was performed on a Leica TCS SP2 AOBS microscope and processed in Adobe Photoshop.

TIRF microscopy was performed using a Leica AM TIRF MC system mounted on a Leica AF 6000 microscope (Leica Microsystems). A 63×/1.40 NA oil-immersion objective was used and laser penetration depth was set at a 110 nm. Excitation and analysis of GFP

fluorescent proteins was performed with a 488nm laser, RFP-proteins with a 532nm laser and CFP-proteins with a 405nm laser. Imaging was recorded on a Hamamatsu Photonics emCCD Camera (C9100-02). Controls were performed transfecting cells with single constructs (either GFP-RN-tre, or RFP-Rab5 or CFP-paxillin) and analysed under the same conditions used for the cells simultaneously transfected with the three constructs, in order to verify the absence of crosstalk among the channels.

FRAP was performed on an UltraVIEW VoX spinning disc confocal system (PerkinElmer), equipped with an EclipseTi inverted microscope (Nikon) provided with a Nikon Perfect Focus System, an integrated FRAP PhotoKinesis unit (PerkinElmer), a C9100-50 emCCD camera (Hamamatsu) and driven by Volocity software (Improvision, Perkin Elmer).

All the experiments were performed using an environmental microscope incubator (OKOLab) set to 37°C and 5% CO_2 perfusion. All images were acquired through a 60× oil immersion objective (Nikon Plan Apo VC, NA 1.4). WT and KO MEF populations, and KO MEF either treated with doxycycline or silenced with siRNA oligos (as described in legend to Figure 4) were transiently transfected, 24 hours before FRAP, with GFP-paxillin. Several bleach regions with a size of 4 × 2.2 μm were positioned on selected peripheral FA or on adhesions at the cell rear. Photobleaching was performed using fifty iterations with the 50 mW solid state 488nm laser set to the maximum power. To determine the recovery kinetics of peripheral adhesions, post-bleaching images were recorded for 200 seconds: the first 150 seconds with a speed of 0.5 frame/sec and then of 0.1 frame/sec. For adhesions at the cell rear, post-bleaching images were recorded with a speed of 0.5 frame/sec for the first 154 seconds and then 0.2 frame/sec. In the case of fibrillar adhesions, which are thin elongated structures, in order to minimise the photobleaching of the GFP-paxillin in the cytoplasm, the size of bleach regions was set to 5 x 1.5 μm and the post-bleaching recovery was recorded for 200 sec: the first 70 seconds with a speed of 1 frame/second and then of 0.3 frame/second.

Quantitative analyses were performed with ImageJ software (http://rsb.info.nih.gov/ij/): the mean intensity values over time were measured, background subtracted and corrected for acquisition photobleaching. A single exponential function was used to fit the recovery curves of peripheral FA and adhesions at the cell rear. For fibrillar adhesions a double exponential fitting was used.

Dunn-chamber assays

Cells were seeded onto a suitably washed sterile coverslip and allowed to settle prior to assembling the chemotaxis chamber. Initially, both annular wells were filled with medium supplemented with 0.5% South American serum and the coverslip seeded with cells was inverted onto the chamber in an offset position in order to leave a narrow filling space at one edge for access to the outer well. The coverslip was sealed in place using hot orthodontic wax applied with a paintbrush around all the edges except for the filling space. The medium in the outer well was replaced with medium containing 10 ng/ml PDGF. The chamber was incubated at 37°C, 5% CO_2 and the images were taken with a Nikon Eclipse TE2000-E inverted microscope.

Integrin internalisation assays

Integrin endocytosis assays were performed as previously described [40]. Briefly, cells were transferred to ice, washed twice in cold phosphate-buffered saline (PBS), and surface-labelled at 4 °C with 0.5 mg/ml sulfo-NHS-SS-biotin (ThermoScientific) in PBS for 30 min. Labelled cells were washed twice with ice-cold DMEM 1% FBS and twice with ice-cold PBS and transferred to pre-warmed DMEM 1% FBS at 37 °C containing 0.2 mM primaquine, an anti-malaria drug known to inhibit recycling of membrane and membrane-bound molecules to the PM from endosomes [51]. At the indicated times, dishes were rapidly transferred to ice and

washed twice with ice-cold PBS. Biotin was removed from proteins remaining at the cell surface by incubation with a solution containing 20 mM sodium 2-mercaptoethanesulfonate (MesNa) in 50 mM Tris-HCl (pH 8.6), 100 mM NaCl, 0.015 N NaOH for 1 h at 4°C. MesNa was quenched by the addition of 20 mM iodoacetamide for 10 min, and after two further washes in PBS, the cells were lysed in 25 mM Tris-HCl, pH 7.6, 100 mM NaCl, 2 mM MgCl2, 1 mM Na3VO4, 0.5 mM EGTA, 1% Triton X-100, 5% glycerol, protease mix (Sigma), and 1 mM PMSF. Lysates were cleared by centrifugation at 12,000g for 20 min. After correction to equivalent protein concentrations, the levels of biotinylated β1-integrin were determined by capture-ELISA as in [40]. Antibodies used in the ELISA assays were: mouse anti-β1-integrin (Abcam, ab30388) or rat anti-active-β1 integrin 9EG7 (BD Pharmingen, 550531).

Further detailed experimental procedures, including expression vectors and antibodies, RNAi silencing, GAP assays, pull down assays for detection of Rab5-GTP, transferrin and EGF saturation binding, and internalisation assays are described in Supplemental Data.

ACKNOWLEDGMENTS

We thank David Lambright for his help with the GAP assays. Work in the authors' lab is supported by grants from the Associazione Italiana per la Ricerca sul Cancro (PPDF, GS and START UP program LL), the European Community (FP7) (PPDF), the European Research Council (PPDF, GS), the Italian Ministries of Education-University-Research (MIUR) and of Health (PPDF and GS), the Association for International Cancer Research (GS and LL), the Ferrari Foundation (PPDF), the Monzino Foundation (PPDF), and the CARIPLO Foundation (PPDF, GS), the Fondazione Piemontese per la Ricerca sul Cancro - ONLUS – Intramural Grant 5X1000 2008 (LL).

REFERENCES

1. Zaidel-Bar, R., Itzkovitz, S., Ma'ayan, A., Iyengar, R., and Geiger, B. (2007). Functional atlas of the integrin adhesome. Nat Cell Biol *9*, 858-867.
2. Parsons, J.T., Horwitz, A.R., and Schwartz, M.A. (2011). Cell adhesion: integrating cytoskeletal dynamics and cellular tension. Nat Rev Mol Cell Biol *11*, 633-643.
3. Ridley, A.J., Schwartz, M.A., Burridge, K., Firtel, R.A., Ginsberg, M.H., Borisy, G., Parsons, J.T., and Horwitz, A.R. (2003). Cell migration: integrating signals from front to back. Science *302*, 1704-1709.
4. Caswell, P.T., and Norman, J.C. (2006). Integrin trafficking and the control of cell migration. Traffic *7*, 14-21.
5. Pellinen, T., Arjonen, A., Vuoriluoto, K., Kallio, K., Fransen, J.A., and Ivaska, J. (2006). Small GTPase Rab21 regulates cell adhesion and controls endosomal traffic of beta1-integrins. J Cell Biol *173*, 767-780.
6. Ezratty, E.J., Bertaux, C., Marcantonio, E.E., and Gundersen, G.G. (2009). Clathrin mediates integrin endocytosis for focal adhesion disassembly in migrating cells. J Cell Biol *187*, 733-747.
7. Valdembri, D., Caswell, P.T., Anderson, K.I., Schwarz, J.P., Konig, I., Astanina, E., Caccavari, F., Norman, J.C., Humphries, M.J., Bussolino, F., et al. (2009). Neuropilin-1/GIPC1 signaling regulates alpha5beta1 integrin traffic and function in endothelial cells. PLoS Biol *7*, e25.
8. Ezratty, E.J., Partridge, M.A., and Gundersen, G.G. (2005). Microtubule-induced focal adhesion disassembly is mediated by dynamin and focal adhesion kinase. Nat Cell Biol *7*, 581-590.
9. Chao, W.T., and Kunz, J. (2009). Focal adhesion disassembly requires clathrin-dependent endocytosis of integrins. FEBS Lett *583*, 1337-1343.
10. Mai, A., Veltel, S., Pellinen, T., Padzik, A., Coffey, E., Marjomäki, V., and Ivaska, J. (2011). Competitive binding of Rab21 and p120RasGAP to integrins regulates receptor traffic and migration. J Cell Biol *194*, 291-306.
11. Zerial, M., and McBride, H. (2001). Rab proteins as membrane organizers. Nat Rev Mol Cell Biol *2*, 107-117.
12. Yuan, L., Fairchild, M.J., Perkins, A.D., and Tanentzapf, G. (2010). Analysis of integrin turnover in fly myotendinous junctions. J Cell Sci *123*, 939-946.
13. Jekely, G., Sung, H.H., Luque, C.M., and Rorth, P. (2005). Regulators of endocytosis maintain localized receptor tyrosine kinase signaling in guided migration. Dev Cell *9*, 197-207.
14. Palamidessi, A., Frittoli, E., Garre, M., Faretta, M., Mione, M., Testa, I., Diaspro, A., Lanzetti, L., Scita, G., and Di Fiore, P.P. (2008). Endocytic trafficking of Rac is required for the spatial restriction of signaling in cell migration. Cell *134*, 135-147.
15. Sigismund, S., Confalonieri, S., Ciliberto, A., Polo, S., Scita, G., and Di Fiore, P.P. (2012). Endocytosis and signaling: cell logistics shape the eukaryotic cell plan. Physiol Rev *92*, 273-366.
16. Stenmark, H. (2009). Rab GTPases as coordinators of vesicle traffic. Nat Rev Mol Cell Biol *10*, 513-525.
17. Frasa, M.A., Koessmeier, K.T., Ahmadian, M.R., and Braga, V.M. (2012). Illuminating the functional and structural repertoire of human TBC/RABGAPs. Nat Rev Mol Cell Biol *13*, 67-73.
18. Lanzetti, L., Rybin, V., Malabarba, M.G., Christoforidis, S., Scita, G., Zerial, M., and Di Fiore, P.P. (2000). The Eps8 protein coordinates EGF receptor signalling through Rac and trafficking through Rab5. Nature *408*, 374-377.

19. Lanzetti, L., Palamidessi, A., Areces, L., Scita, G., and Di Fiore, P.P. (2004). Rab5 is a signalling GTPase involved in actin remodelling by receptor tyrosine kinases. Nature *429*, 309-314.
20. Haas, A.K., Fuchs, E., Kopajtich, R., and Barr, F.A. (2005). A GTPase-activating protein controls Rab5 function in endocytic trafficking. Nat Cell Biol *7*, 887-893.
21. Fuchs, E., Haas, A.K., Spooner, R.A., Yoshimura, S., Lord, J.M., and Barr, F.A. (2007). Specific Rab GTPase-activating proteins define the Shiga toxin and epidermal growth factor uptake pathways. J Cell Biol *177*, 1133-1143.
22. Haas, A.K., Yoshimura, S., Stephens, D.J., Preisinger, C., Fuchs, E., and Barr, F.A. (2007). Analysis of GTPase-activating proteins: Rab1 and Rab43 are key Rabs required to maintain a functional Golgi complex in human cells. J Cell Sci *120*, 2997-3010.
23. Dejgaard, S.Y., Murshid, A., Erman, A., Kizilay, O., Verbich, D., Lodge, R., Dejgaard, K., Ly-Hartig, T.B., Pepperkok, R., Simpson, J.C., et al. (2008). Rab18 and Rab43 have key roles in ER-Golgi trafficking. J Cell Sci *121*, 2768-2781.
24. Rämet, M., Manfruelli, P., Pearson, A., Mathey-Prevot, B., and Ezekowitz, R.A. (2002). Functional genomic analysis of phagocytosis and identification of a Drosophila receptor for E. coli. Nature *416*, 644-648.
25. Scholpp, S., and Brand, M. (2004). Endocytosis controls spreading and effective signaling range of Fgf8 protein. Curr Biol *14*, 1834-1841.
26. Buccione, R., Orth, J.D., and McNiven, M.A. (2004). Foot and mouth: podosomes, invadopodia and circular dorsal ruffles. Nat Rev Mol Cell Biol *5*, 647-657.
27. Schiller, H.B., Friedel, C.C., Boulegue, C., and Fässler, R. (2011). Quantitative proteomics of the integrin adhesome show a myosin II-dependent recruitment of LIM domain proteins. EMBO Rep *12*, 259-266.
28. Kuo, J.C., Han, X., Hsiao, C.T., Yates Iii, J.R., and Waterman, C.M. (2011). Analysis of the myosin-II-responsive focal adhesion proteome reveals a role for beta-Pix in negative regulation of focal adhesion maturation. Nat Cell Biol *13*, 383-393.
29. Lanzetti, L., Margaria, V., Melander, F., Virgili, L., Lee, M.H., Bartek, J., and Jensen, S. (2007). Regulation of the Rab5 GTPase-activating protein RN-tre by the dual specificity phosphatase Cdc14A in human cells. J Biol Chem *282*, 15258-15270.
30. Bazzoni, G., Shih, D.T., Buck, C.A., and Hemler, M.E. (1995). Monoclonal antibody 9EG7 defines a novel beta 1 integrin epitope induced by soluble ligand and manganese, but inhibited by calcium. J Biol Chem *270*, 25570-25577.
31. Clark, K., Pankov, R., Travis, M.A., Askari, J.A., Mould, A.P., Craig, S.E., Newham, P., Yamada, K.M., and Humphries, M.J. (2005). A specific {alpha}5{beta}1-integrin conformation promotes directional integrin translocation and fibronectin matrix formation 10.1242/jcs.01623. J Cell Sci *118*, 291-300.
32. Pankov, R., Cukierman, E., Katz, B.-Z., Matsumoto, K., Lin, D.C., Lin, S., Hahn, C., and Yamada, K.M. (2000). Integrin Dynamics and Matrix Assembly: Tensin-dependent Translocation of {alpha}5{beta}1 Integrins Promotes Early Fibronectin Fibrillogenesis. J. Cell Biol. *148*, 1075-1090.
33. Pan, X., Eathiraj, S., Munson, M., and Lambright, D.G. (2006). TBC-domain GAPs for Rab GTPases accelerate GTP hydrolysis by a dual-finger mechanism. Nature *442*, 303-306.
34. Simon, I., Zerial, M., and Goody, R.S. (1996). Kinetics of interaction of Rab5 and Rab7 with nucleotides and magnesium ions. J Biol Chem *271*, 20470-20478.
35. Rybin, V., Ullrich, O., Rubino, M., Alexandrov, K., Simon, I., Seabra, M.C., Goody, R., and Zerial, M. (1996). GTPase activity of Rab5 acts as a timer for endocytic membrane fusion. Nature *383*, 266-269.

36. Simonsen, A., Lippe, R., Christoforidis, S., Gaullier, J.M., Brech, A., Callaghan, J., Toh, B.H., Murphy, C., Zerial, M., and Stenmark, H. (1998). EEA1 links PI(3)K function to Rab5 regulation of endosome fusion. Nature *394*, 494-498.
37. Christoforidis, S., McBride, H.M., Burgoyne, R.D., and Zerial, M. (1999). The Rab5 effector EEA1 is a core component of endosome docking. Nature *397*, 621-625.
38. Barbieri, M.A., Roberts, R.L., Gumusboga, A., Highfield, H., Alvarez-Dominguez, C., Wells, A., and Stahl, P.D. (2000). Epidermal growth factor and membrane trafficking. EGF receptor activation of endocytosis requires Rab5a. J Cell Biol *151*, 539-550.
39. Ginsberg, M.H., Partridge, A., and Shattil, S.J. (2005). Integrin regulation. Curr Opin Cell Biol *17*, 509-516.
40. Roberts, M., Barry, S., Woods, A., van der Sluijs, P., and Norman, J. (2001). PDGF-regulated rab4-dependent recycling of alphavbeta3 integrin from early endosomes is necessary for cell adhesion and spreading. Curr Biol *11*, 1392-1402.
41. Pasapera, A.M., Schneider, I.C., Rericha, E., Schlaepfer, D.D., and Waterman, C.M. (2010). Myosin II activity regulates vinculin recruitment to focal adhesions through FAK-mediated paxillin phosphorylation. J Cell Biol *188*, 877-890.
42. Zeigerer, A., Gilleron, J., Bogorad, R.L., Marsico, G., Nonaka, H., Seifert, S., Epstein-Barash, H., Kuchimanchi, S., Peng, C.G., Ruda, V.M., et al. (2012). Rab5 is necessary for the biogenesis of the endolysosomal system in vivo. Nature *485*, 465-470.
43. Teckchandani, A., Toida, N., Goodchild, J., Henderson, C., Watts, J., Wollscheid, B., and Cooper, J.A. (2009). Quantitative proteomics identifies a Dab2/integrin module regulating cell migration. The Journal of Cell Biology *186*, 99-111.
44. Caswell, P.T., Vadrevu, S., and Norman, J.C. (2009). Integrins: masters and slaves of endocytic transport. Nat Rev Mol Cell Biol *10*, 843-853.
45. Laukaitis, C.M., Webb, D.J., Donais, K., and Horwitz, A.F. (2001). Differential Dynamics of {alpha}5 Integrin, Paxillin, and {alpha}-Actinin during Formation and Disassembly of Adhesions in Migrating Cells 10.1083/jcb.153.7.1427. J. Cell Biol. *153*, 1427-1440.
46. Laflamme, C., Assaker, G., Ramel, D., Dorn, J.F., She, D., Maddox, P.S., and Emery, G. (2012). Evi5 promotes collective cell migration through its Rab-GAP activity. J Cell Biol *198*, 57-67.
47. Assaker, G., Ramel, D., Wculek, S.K., González-Gaitán, M., and Emery, G. (2010). Spatial restriction of receptor tyrosine kinase activity through a polarized endocytic cycle controls border cell migration. Proc Natl Acad Sci U S A *107*, 22558-22563.
48. Sandri, C., Caccavari, F., Valdembri, D., Camillo, C., Veltel, S., Santambrogio, M., Lanzetti, L., Bussolino, F., Ivaska, J., and Serini, G. (2012). The R-Ras/RIN2/Rab5 complex controls endothelial cell adhesion and morphogenesis via active integrin endocytosis and Rac signaling. Cell Res *22*, 1479-1501.
49. Levéen, P., Pekny, M., Gebre-Medhin, S., Swolin, B., Larsson, E., and Betsholtz, C. (1994). Mice deficient for PDGF B show renal, cardiovascular, and hematological abnormalities. Genes Dev *8*, 1875-1887.
50. Serio, G., Margaria, V., Jensen, S., Oldani, A., Bartek, J., Bussolino, F., and Lanzetti, L. (2011). Small GTPase Rab5 participates in chromosome congression and regulates localization of the centromere-associated protein CENP-F to kinetochores. Proc Natl Acad Sci U S A *108*, 17337-17342.
51. van Weert, A.W., Geuze, H.J., Groothuis, B., and Stoorvogel, W. (2000). Primaquine interferes with membrane recycling from endosomes to the plasma membrane through

a direct interaction with endosomes which does not involve neutralisation of endosomal pH nor osmotic swelling of endosomes. Eur J Cell Biol *79*, 394-399.

52. Foxman, E.F., Kunkel, E.J., and Butcher, E.C. (1999). Integrating conflicting chemotactic signals. The role of memory in leukocyte navigation. J Cell Biol *147*, 577-588.

FIGURE LEGENDS

Figure 1. RN-tre is in adhesive sites.

(A) TIRF microscopy of MEF expressing, in the upper panel, GFP-RN-tre (green in merge) and RFP-vinculin (red in merge) and, in the bottom panel, cherry-RN-tre (red in merge) and GFP-paxillin (green in merge). (B) Confocal analysis of MEF expressing GFP-RN-tre (green), stained with a conformation-specific antibody that recognizes the active form of β1-integrin (9EG7, red). Co-localisation resulting in yellow staining is evident in the merged image (GFP-RN-tre+9EG7). Cells were also stained with Alexa Fluor 647-conjugated phalloidin (shown in magenta in merge). Regions of cell corresponding to FA (a) or fibrillar adhesions (b) were magnified in the insets. Bar, 10 μm.

Figure 2. RN-tre is a Rab5-GAP.

(A-C) RN-tre and RabGAP-5 display the same GAP catalytic efficiency toward Rab5. Left: time courses of GTP hydrolysis of 20 μM of Rab5 in the absence and presence of various concentrations of TBC domains of RN-tre or of RabGAP-5 (A) or the respective full length proteins (B) (μM concentrations expressed as are shown on the bottom of each graph). Solid lines represent a simultaneously fitted pseudo-first-order Michaelis–Menten model function (see Supplemental Experimental Procedures). Right: the catalytic efficiencies expressed as Kcat/Km of various independent experiments is shown. The value of Kcat/Km of the TBC domains or the full-length proteins for Rab5 were calculated as described in Supplemental Experimental Procedures and summarised in (C). (D) Total cellular lysates from 293T cell transfected with the indicated constructs (CTR, mock transfection) were incubated with GST-EEA1 (GST-EEA1 lanes). Input lysates (50 μg) are also shown. (E) Input lysates of *RN-tre* KO PEF transfected with CFP-Rab5 and stimulated with PDGF for the indicated time were

subjected to GST-EEA1 assay and IB, as indicated. (F) Input lysates of WT or *RN-tre* KO PEF transfected with CFP-Rab5 and stimulated with PDGF for 7 min., as shown on top, were subjected to GST-EEA1 assay and IB, as indicated. (G) *RN-tre* KO MEF stably expressing empty vector (KO), or RN-tre (KO+RN-tre) or RN-tre^{R150A} (KO+RN-treR150A) were transfected with CFP-Rab5 before PDGF (+) or mock (-) stimulation for 7 min. Input lysates were subjected to GST-EEA1 assay and IB, as indicated. Densitometric quantification of Rab5-GTP in (F) and (G) is shown below each panel. Notably, the same amounts of ectopically expressed CFP-Rab5, as witnessed by its levels detected in input lysates by immunoblotting, were used in all these assays.

Figure 3. RN-tre participates in integrin endocytosis and co-localises with Rab5 in proximity of FA undergoing remodelling.

(A-B) RN-tre participates in β1-integrin endocytosis. (A) Bar graph showing the amount of total (black bars) and active (white bars) β1-integrin at the plasma membrane at 4°C in *RN-tre* KO and WT MEF measured by ELISA assays (n = 3 mean values ± SD). (B) *RN-tre* KO and WT MEF were surface labelled with cleavable biotin. Integrin internalisation was allowed for the indicated times and biotin present on the cell surface was cleaved. The amount of biotinylated intracellular total (graph on the left) or active (graph on the right) β1-integrin was determined with ELISA. The data are expressed as the percentage of internalised receptor, relative to the total amount of cell surface–labelled β1-integrin (n = 3, means ± SD; p values < 0.002). (C) Still images from Movie S1 showing TIRF imaging of *RN-tre* KO MEF expressing GFP-RN-tre, RFP-Rab5 and CFP-paxillin. Merged images are also shown. Rab5 and RN-tre co-localise on a pool of vesicles closely associated with remodelling adhesions. Bar, 10 μm.

Figure 4. RN-tre and Rab5 control FA turnover.

RN-tre WT and KO MEF (A-C), KO MEF expressing or not RN-tre or RN-treR^{150A} (D) or KO MEF silenced with Rab5A, B, C or Rab43 or control oligos (CTR) (E) were transfected with GFP-paxillin. GFP-paxillin positive adhesions, in the various cell populations, were subjected to FRAP analysis and the results showing the half time of fluorescence recovery are reported in the box plots. N is the number of FA analysed in each sample. The mean FRAP t1/2 in sec is indicated above each box; **$p < 0.001$. Sample fluorescence recovery curves of FRAP are shown below each plot in (A-C) or reported on the right in (D) and (E). The fluorescence intensity in the recovery curves corresponds to the fluorescence at each time point after photobleaching, background subtracted, and normalised to the pre-bleaching intensity of 1. (A) FRAP of Peripheral FA, (B) FRAP of adhesions at the cell rear, (C) FRAP of fibrillar adhesions. (D) FRAP analysis of GFP-paxillin peripheral FA in *RN-tre* KO MEF expressing the inducible empty vector (KO), or RN-tre (KO+RN-tre) or RN-tre^{R150A} (KO+RN-treR150A). (E) FRAP analysis of GFP-paxillin peripheral FA in *RN-tre* KO MEF silenced with control oligos (CTR) or with oligos for Rab5 (Rab5-KD) or for Rab43 (Rab43-KD). RNAi-interfered cells were analysed for mRNA content by QRT-PCR (Fig. S4A-C).

Figure 5. RN-tre regulates cell motility and chemotactic migration through its GAP activity on Rab5.

(A) PEF derived from *RN-tre* WT or KO littermate embryos were analysed in Dunn chamber assays in the absence of any diffusible gradient. Random cell migration was tracked every 5 minutes interval over 16 hours period. The migratory tracks of some representative cells are shown for WT and KO PEF. Tracking of cells was performed by using the “Manual tracking” and “chemotaxis and migration tool” plugin distributed by ImageJ software. Various migration parameters obtained by monitoring at least 30 single cells/experiment/genotype are

plotted in the graphs below; **p < 0.01. (B) *RN-tre* KO MEF expressing or not RN-tre or RN-tre^{R150A} were analysed for chemotactic migration over a diffusible PDGF gradient in Dunn chamber assays. The migratory tracks of some representative KO, KO+RN-tre and KO+RN-treR150A MEF were determined, as described above. Migration parameters of at least 60 single cells/experiment/condition are plotted in the graphs below. The forward migration index represents the efficiency of forward migration of cells on the axis parallel to the direction (indicated by the arrow) of a chemotactic gradient. It is calculated by dividing the net distance covered by a cell in the direction of the chemotactic migration axis (Xc) per the total accumulated distance (Dc), as described in [52]. (C) KO MEF were transfected with Rab5A, B, C, or Rab43 or Rab30 or scrambled RNAi (used as control, CTR, Fig. S4A-C) and subjected to Dunn chamber assays, as described in (B). The migratory tracks of representative control and Rab-interfered MEF are shown. Various migration parameters obtained by monitoring at least 50 single cells/experiment are plotted in the graphs below; **p < 0.01.

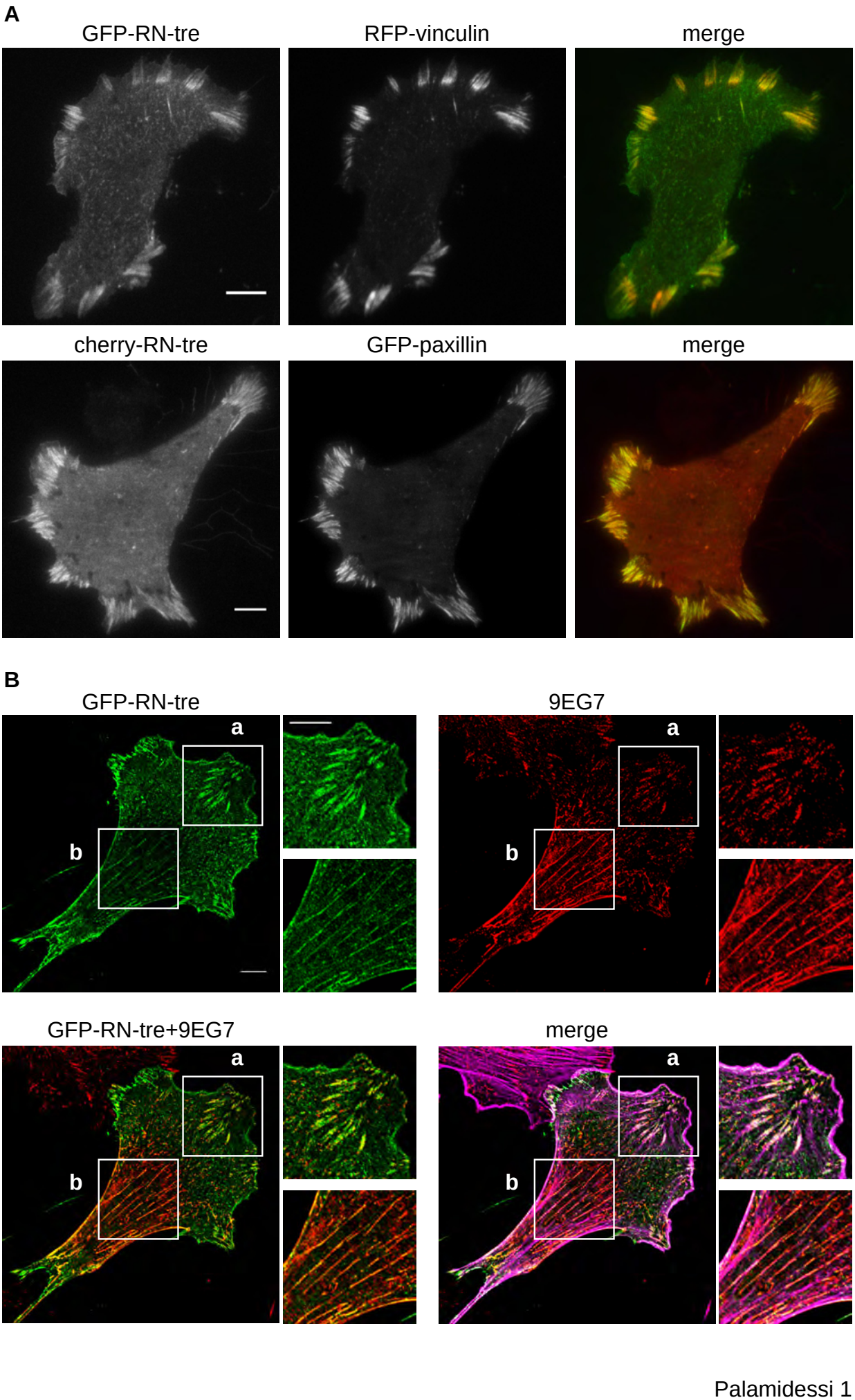
A
GFP-RN-tre
RFP-vinculin
merge
cherry-RN-tre
GFP-paxillin
merge
B
GFP-RN-tre
9EG7
a
b
GFP-RN-tre+9EG7
merge

Figure

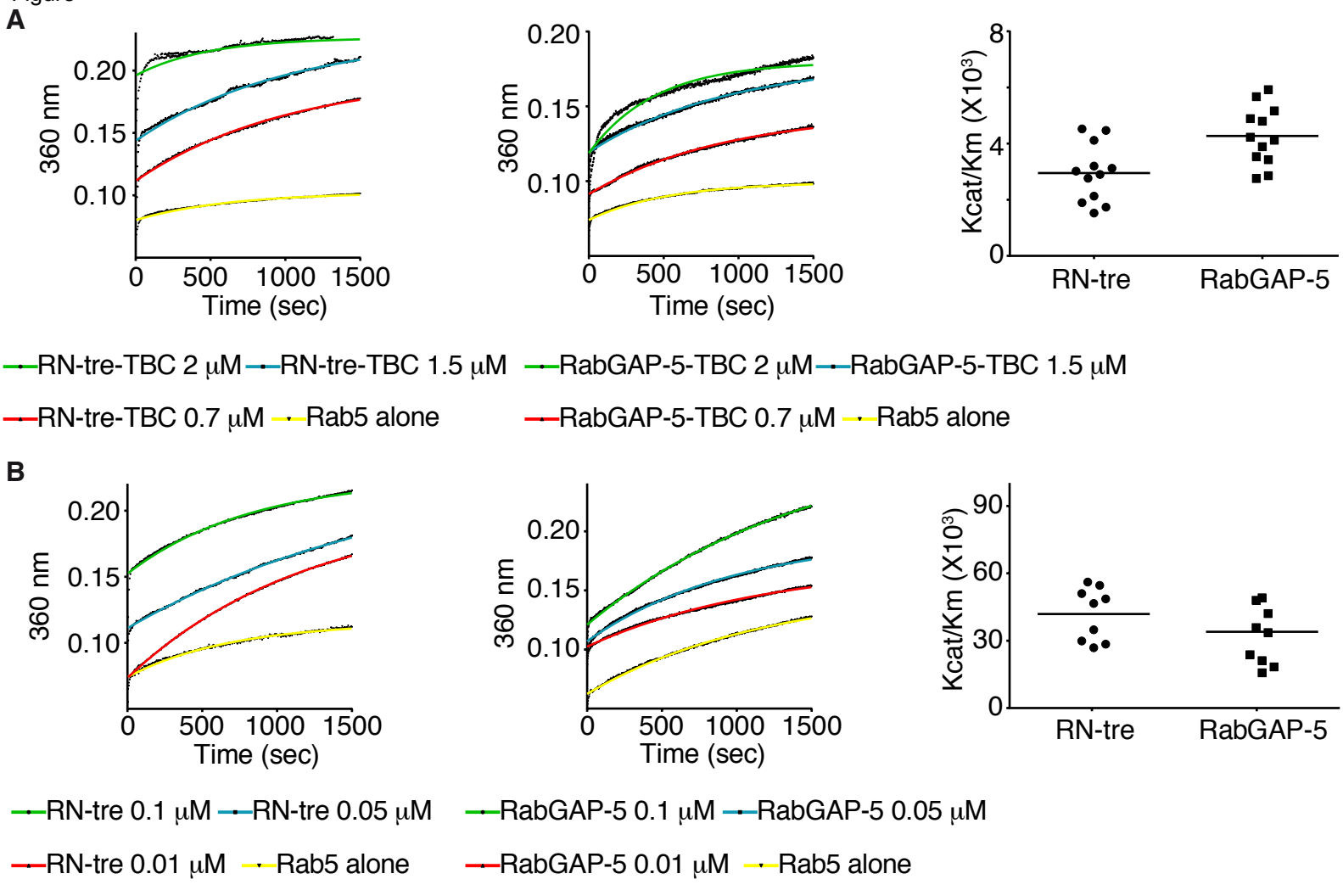

C

Kcat/Km (M^{-1} s^{-1})			
RN-tre TBC	RabGAP-5 TBC	RN-tre FL	RabGAP-5 FL
2.9×10^3	4.2×10^3	4.2×10^4	3.4×10^4

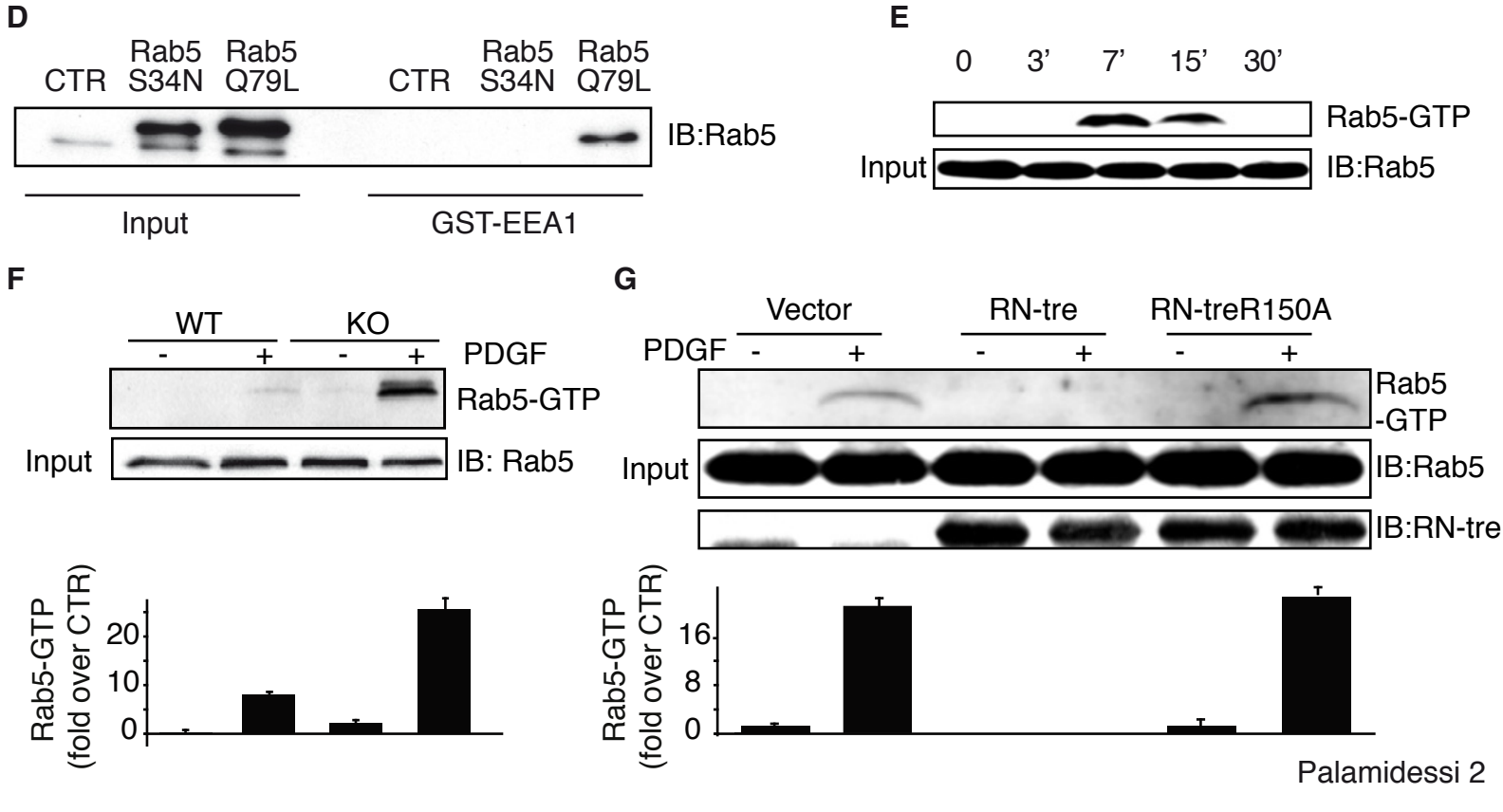

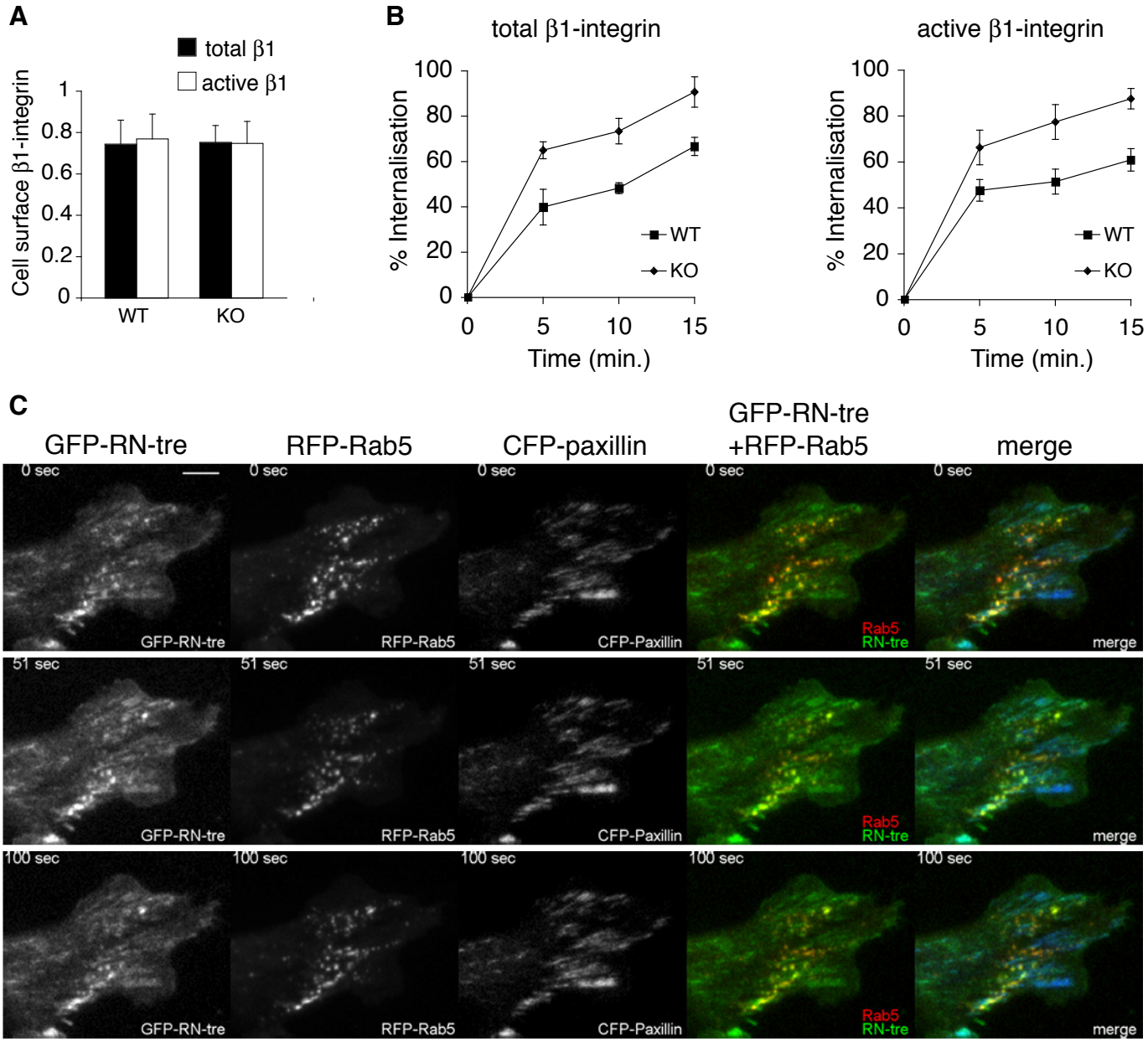
A
total β1
active β1
Cell surface β1-integrin
1
0.8
0.6
0.4
0.2
0
WT
KO
B
total β1-integrin
% Internalisation
100
80
60
40
20
0
0
5
10
15
Time (min.)
WT
KO
active β1-integrin
% Internalisation
100
80
60
40
20
0
0
5
10
15
Time (min.)
WT
KO
C
GFP-RN-tre
RFP-Rab5
CFP-paxillin
GFP-RN-tre +RFP-Rab5
merge
0 sec
51 sec
100 sec
GFP-RN-tre
RFP-Rab5
CFP-Paxillin
Rab5
RN-tre
merge

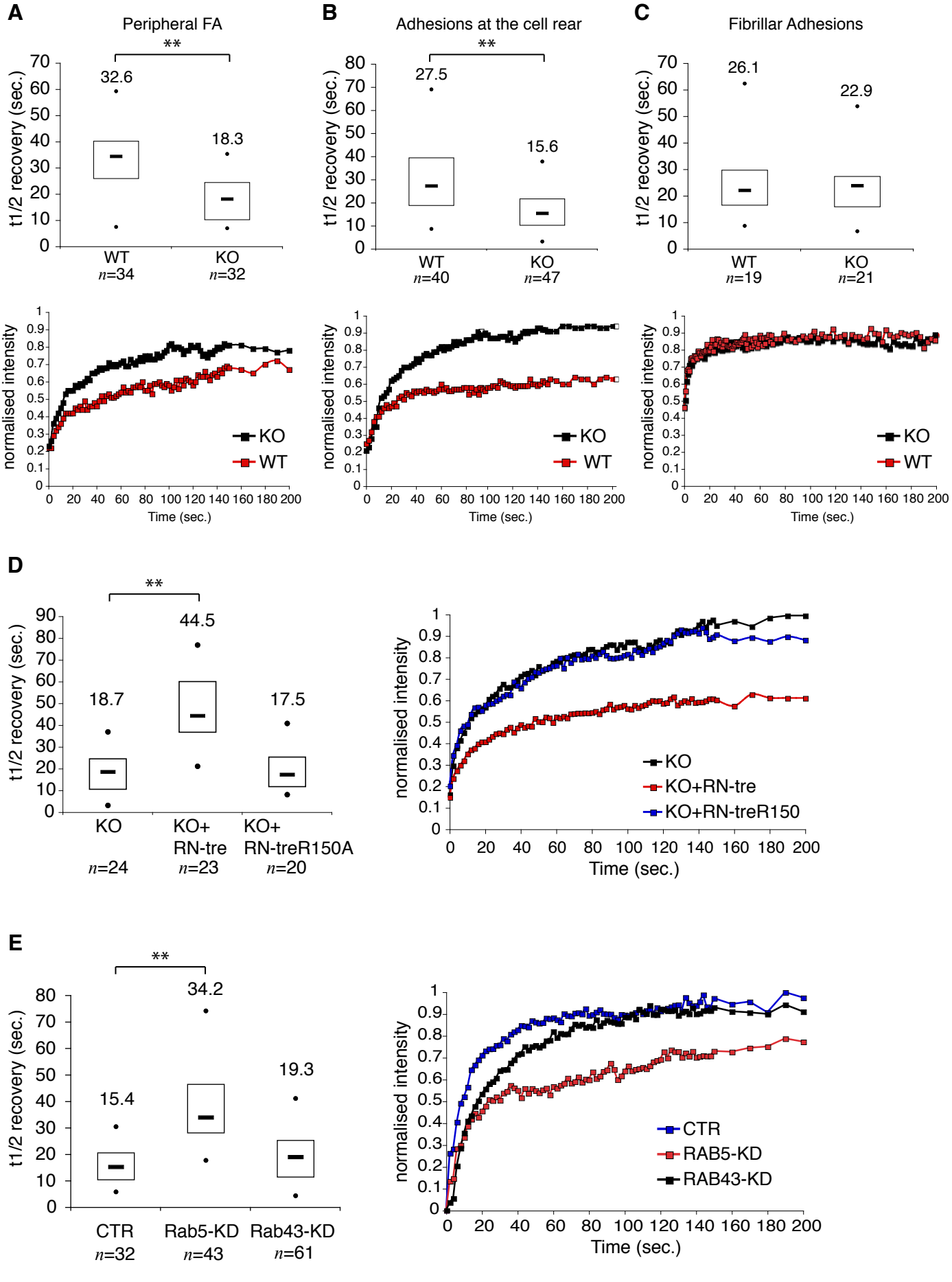
A
Peripheral FA
**
32.6
18.3
t1/2 recovery (sec.)
WT
n=34
KO
n=32
B
Adhesions at the cell rear
**
27.5
15.6
t1/2 recovery (sec.)
WT
n=40
KO
n=47
C
Fibrillar Adhesions
26.1
22.9
t1/2 recovery (sec.)
WT
n=19
KO
n=21
normalised intensity
KO
WT
Time (sec.)
D
**
44.5
18.7
17.5
t1/2 recovery (sec.)
KO
n=24
KO+
RN-tre
n=23
KO+
RN-treR150A
n=20
normalised intensity
KO
KO+RN-tre
KO+RN-treR150
Time (sec.)
E
**
34.2
19.3
15.4
t1/2 recovery (sec.)
CTR
n=32
Rab5-KD
n=43
Rab43-KD
n=61
normalised intensity
CTR
RAB5-KD
RAB43-KD
Time (sec.)

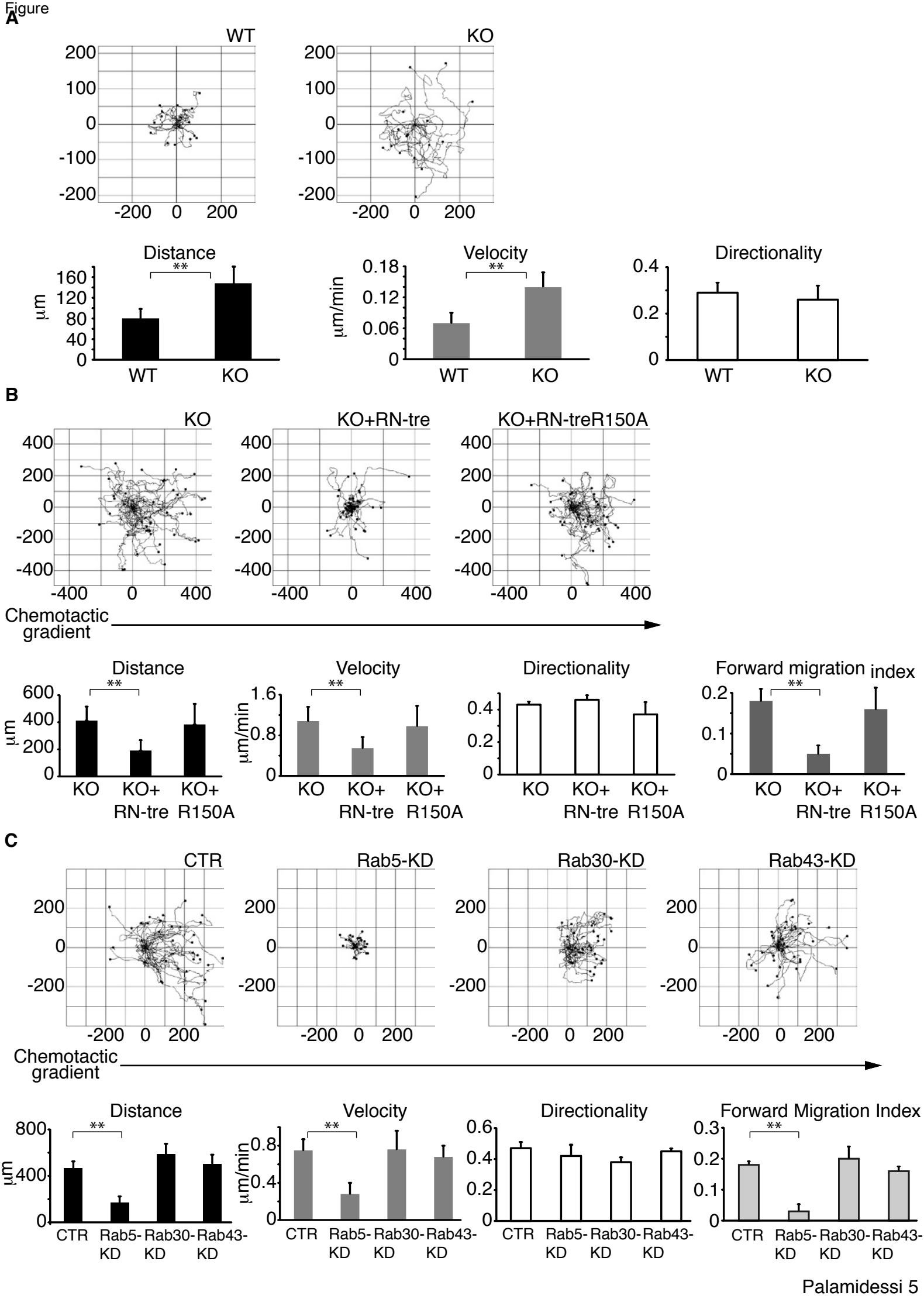
A
WT
KO
200
100
0
-100
-200
-200 0 200
Distance
**
μm
160
120
80
40
0
WT KO
Velocity
**
μm/min
0.18
0.12
0.06
0
WT KO
Directionality
0.4
0.2
0
WT KO
B
KO
KO+RN-tre
KO+RN-treR150A
400
200
0
-200
-400
-400 0 400
Chemotactic gradient
Distance
**
μm
600
400
200
0
KO KO+ RN-tre KO+ R150A
Velocity
**
μm/min
1.6
0.8
0
KO KO+ RN-tre KO+ R150A
Directionality
0.4
0.2
0
KO KO+ RN-tre KO+ R150A
Forward migration index
**
0.2
0.1
0
KO KO+ RN-tre KO+ R150A
C
CTR
Rab5-KD
Rab30-KD
Rab43-KD
200
0
-200
-200 0 200
Chemotactic gradient
Distance
**
μm
800
400
0
CTR Rab5-KD Rab30-KD Rab43-KD
Velocity
**
μm/min
0.8
0.4
0
CTR Rab5-KD Rab30-KD Rab43-KD
Directionality
0.6
0.4
0.2
0
CTR Rab5-KD Rab30-KD Rab43-KD
Forward Migration Index
**
0.3
0.2
0.1
0
CTR Rab5-KD Rab30-KD Rab43-KD

Inventory of Supplemental Information

1 Supplemental Figures

2 Supplemental Movies

Movie S1. TIRF analysis of GFP-RN-tre, RFP-Rab5 and CFP-paxillin. Related to Figure 3.

Movie S2. FRAP analysis of GFP-paxillin turnover in peripheral FA in WT and KO MEF. Related to Figure 4.

Movie S3. FRAP analysis of GFP-paxillin turnover in adhesions at the cell rear in WT and KO MEF. Related to Figure 4.

Movie S4. FRAP analysis of GFP-paxillin turnover in fibrillar adhesions in WT and KO MEF. Related to Figure 4.

Movie S5. FRAP analysis of GFP-paxillin turnover in *RN-tre* KO MEF re-expressing RN-tre or its GAP-defective mutant. Related to Figure 4.

Movie S6. FRAP analysis of GFP-paxillin in Rab-silenced *RN-tre* KO MEF. Related to Figure 4.

Movie S7. Random motility assay on *RN-tre* WT and KO PEF. Related to Figure 5.

Movie S8. Chemotaxis assay of *RN-tre* KO inducible MEF. Related to Figure 5.

Movie S9. Chemotaxis assay of *RN-tre* KO MEF plated on fibronectin. Related to Figure 5.

Movie S10. Chemotaxis assay of *RN-tre* KO MEF plated on vitronectin. Related to Figure 5.

Movie S11. Chemotaxis assay of HeLa cells overexpressing GFP-RN-tre. Related to Figure 5.

Movie S12. Chemotaxis assay on *RN-tre* KO MEF subjected to siRNA for Rab5, Rab30 and Rab43. Related to Figure 5.

3 Supplemental Experimental Procedures

4 Supplemental References

SUPPLEMENTAL DATA

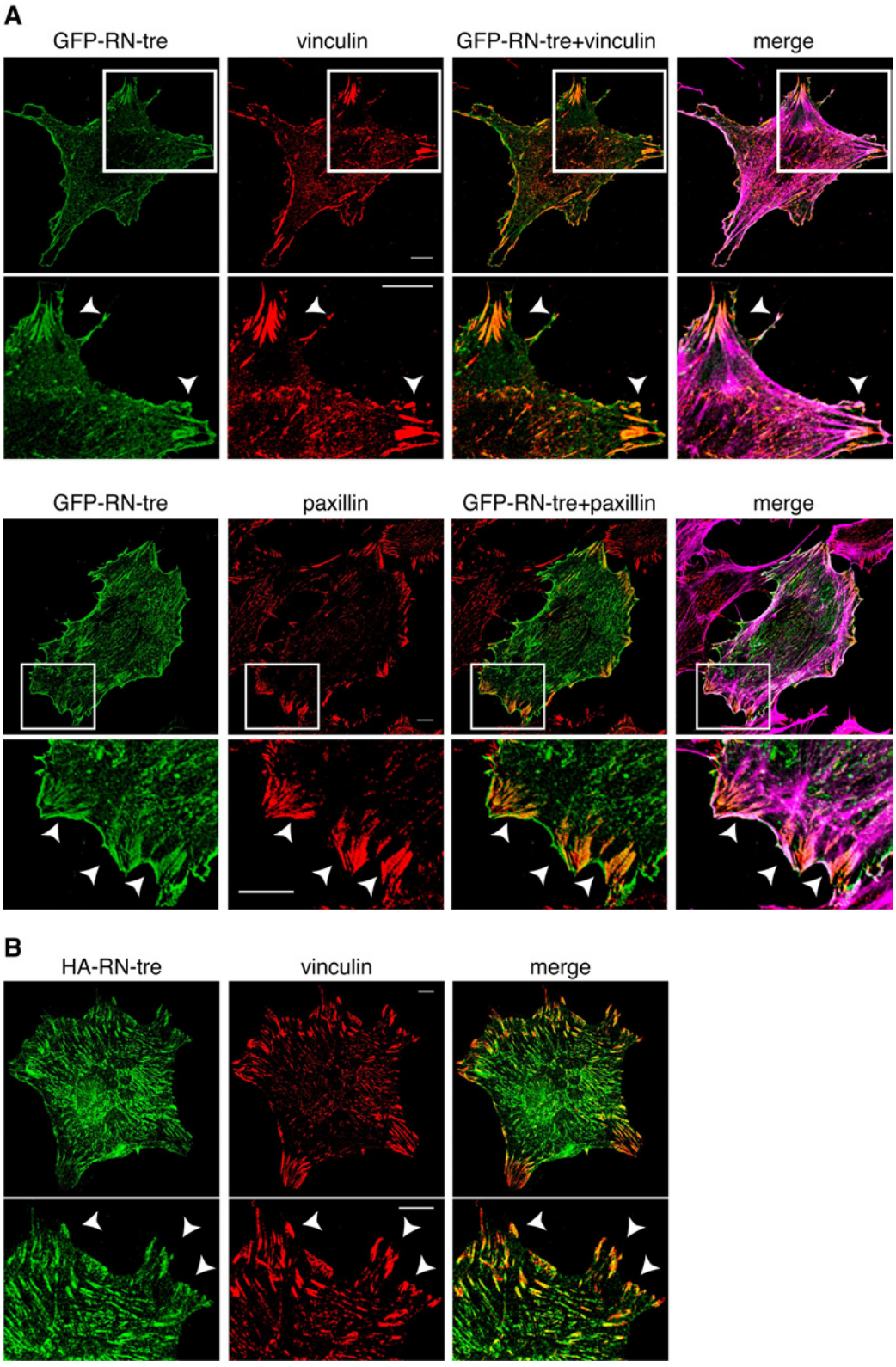

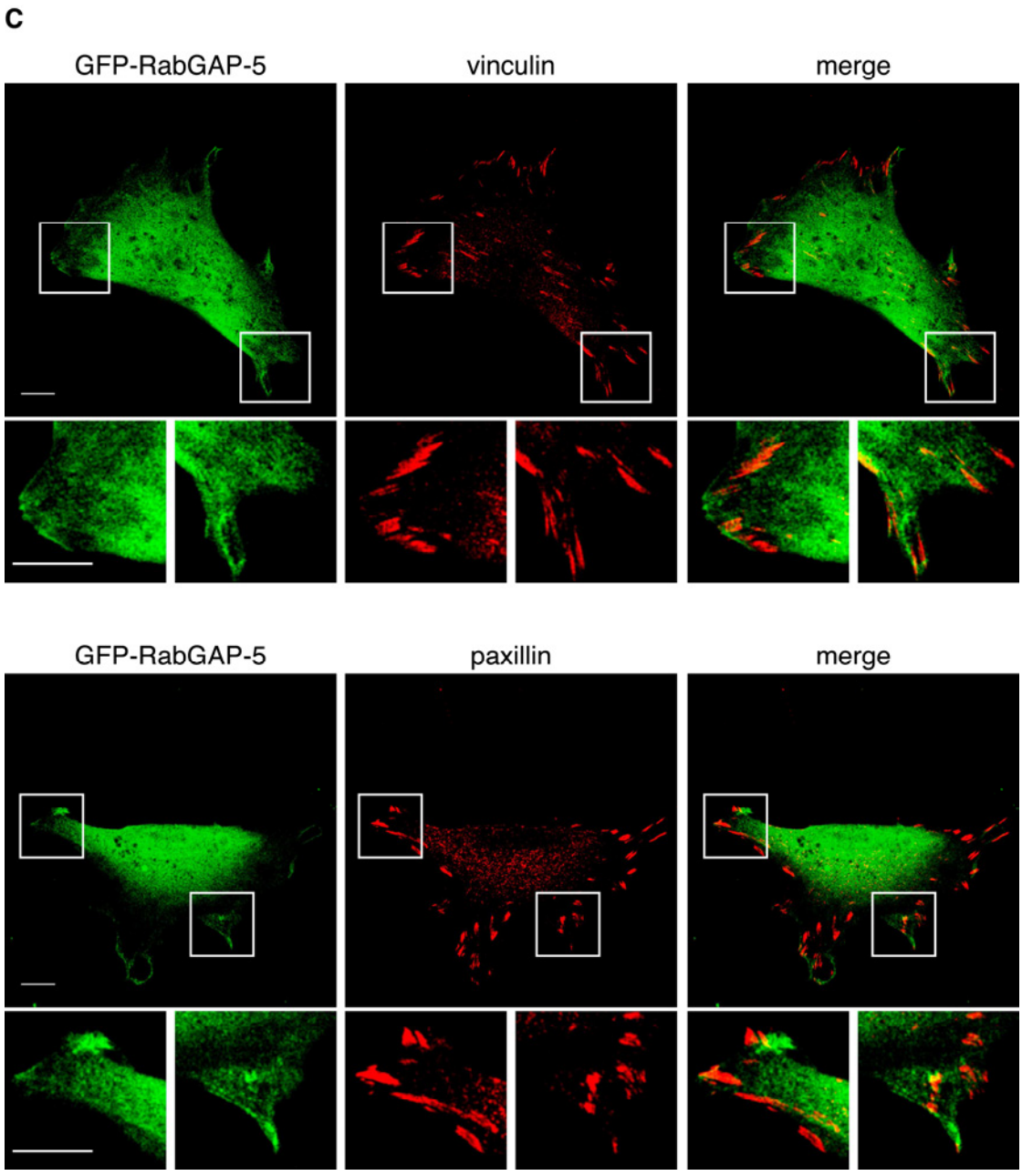

Figure S1, related to Figure 1. RN-tre, but not RabGAP-5, localises to focal adhesions.

(A) Confocal images of MEF expressing GFP-RN-tre (green) stained with antibodies for the adhesive markers vinculin (in red in the top panel) or paxillin (in red in the bottom panel). Co-localisation resulting in yellow staining is evident in the merged images (GFP-RN-tre + vinculin and GFP-RN-tre + paxillin). Cells were also stained with Alexa Fluor 647-

conjugated phalloidin (shown in magenta in the merge). Regions of cells were boxed and magnified in the panels below. Arrowheads point at FA. Bar, 10 μm. (B) Confocal images of MEF expressing HA-RN-tre stained with anti-HA (green) and anti-vinculin (red) antibodies. Co-localization resulting in yellow staining is evident in the merge. A portion of the cell is boxed and magnified in the panels below. Arrowheads point at FA. Bar, 10 μm. (C) Confocal images of MEF expressing GFP-RabGAP-5 (green) stained with antibodies for the adhesive markers vinculin (in red in the top panel) or paxillin (in red in the bottom panel). Merged images are also shown. Regions of cells were boxed and magnified in the panels below. Bar, 10 μm.

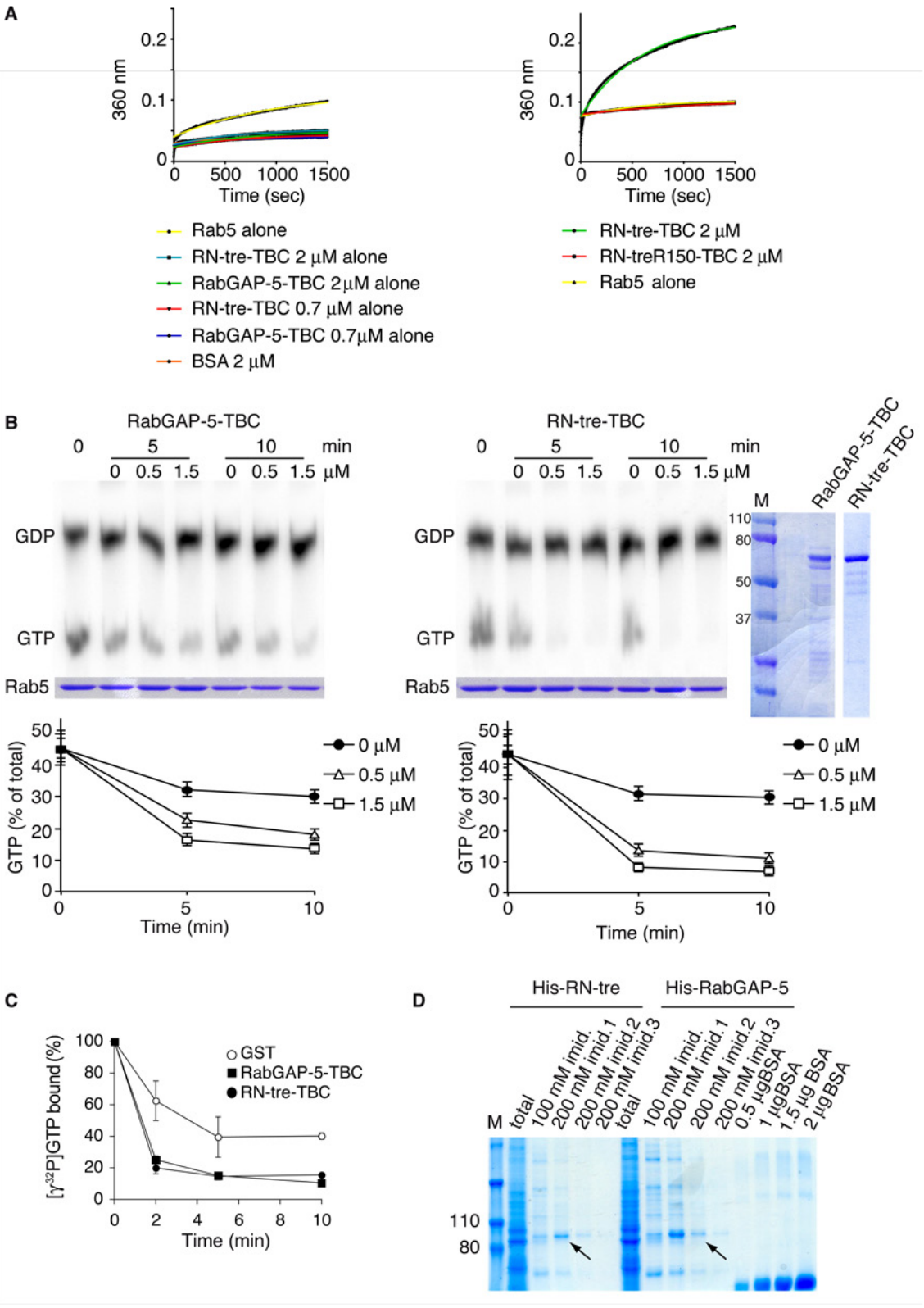
A
360 nm
Time (sec)
Rab5 alone
RN-tre-TBC 2 μM alone
RabGAP-5-TBC 2μM alone
RN-tre-TBC 0.7 μM alone
RabGAP-5-TBC 0.7μM alone
BSA 2 μM
RN-tre-TBC 2 μM
RN-treR150-TBC 2 μM
Rab5 alone
B
RabGAP-5-TBC
RN-tre-TBC
min
μM
GDP
GTP
Rab5
M
RabGAP-5-TBC
RN-tre-TBC
GTP (% of total)
Time (min)
0 μM
0.5 μM
1.5 μM
C
[γ-32P]GTP bound (%)
GST
RabGAP-5-TBC
RN-tre-TBC
Time (min)
D
His-RN-tre
His-RabGAP-5
M
total
100 mM imid.
200 mM imid.1
200 mM imid.2
200 mM imid.3
0.5 μgBSA
1 μgBSA
1.5 μg BSA
2 μgBSA

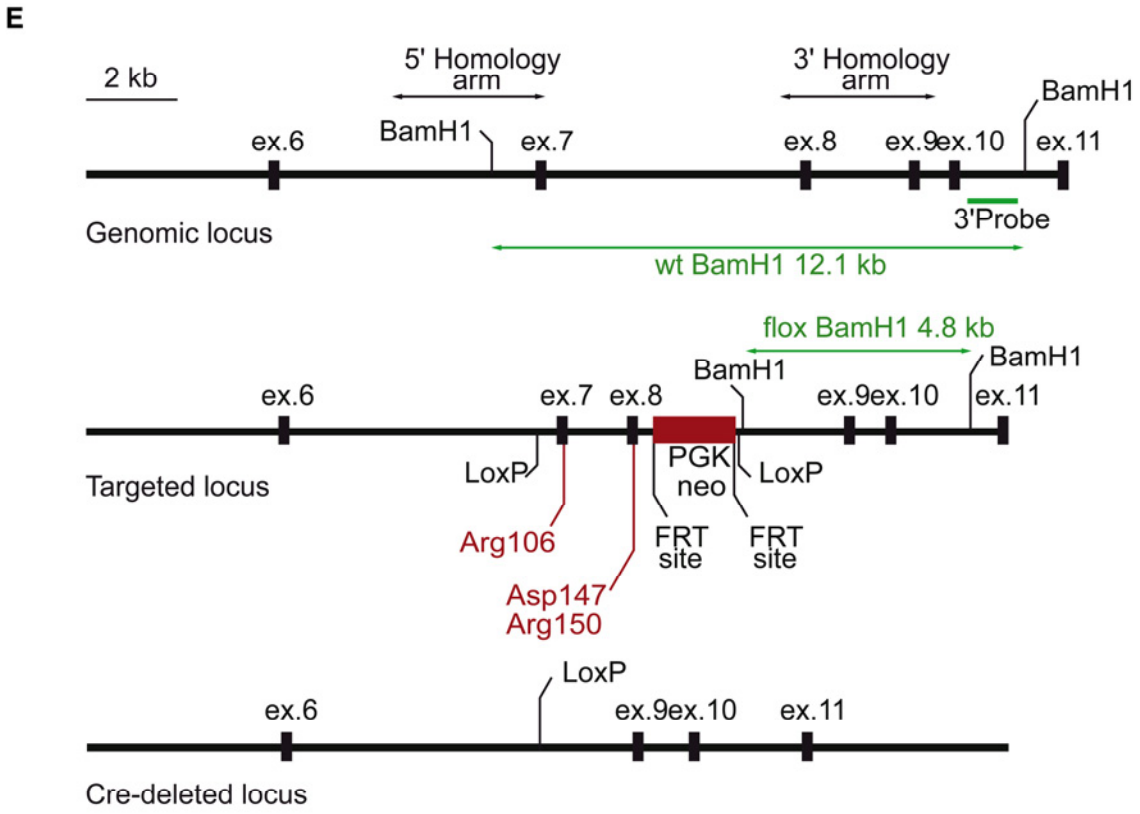
E
2 kb
5' Homology arm
3' Homology arm
BamH1
ex.6
BamH1
ex.7
ex.8
ex.9ex.10
ex.11
3'Probe
Genomic locus
wt BamH1 12.1 kb
flox BamH1 4.8 kb
BamH1
BamH1
ex.6
ex.7
ex.8
ex.9ex.10
ex.11
LoxP
PGK
neo
LoxP
Targeted locus
Arg106
FRT site
FRT site
Asp147
Arg150
LoxP
ex.6
ex.9ex.10
ex.11
Cre-deleted locus

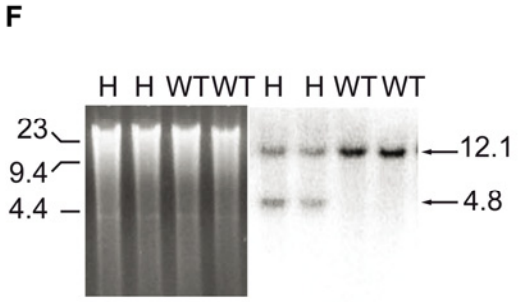
F
H H WT WT H H WT WT
23
9.4
4.4
12.1
4.8

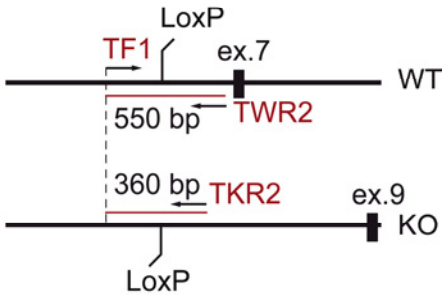
H
LoxP
TF1
ex.7
WT
550 bp
TWR2
360 bp
TKR2
ex.9
KO
LoxP

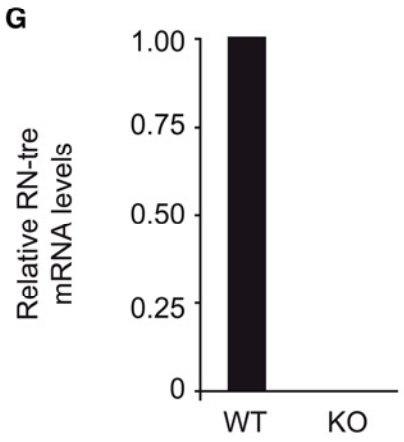
G
Relative RN-tre mRNA levels
1.00
0.75
0.50
0.25
0
WT
KO

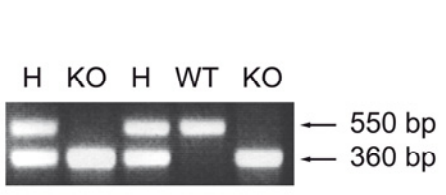
I
H KO H WT KO
550 bp
360 bp

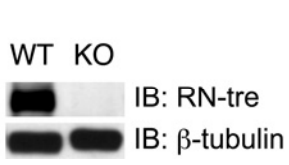
L
WT KO
IB: RN-tre
IB: β-tubulin

M

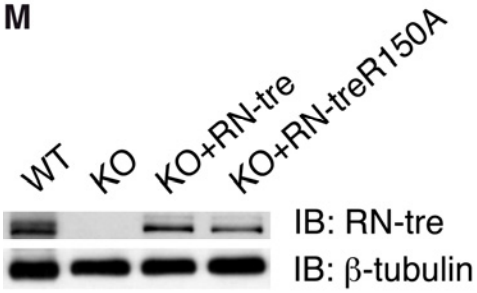
WT
KO
KO+RN-tre
KO+RN-treR150A
IB: RN-tre
IB: β-tubulin

N

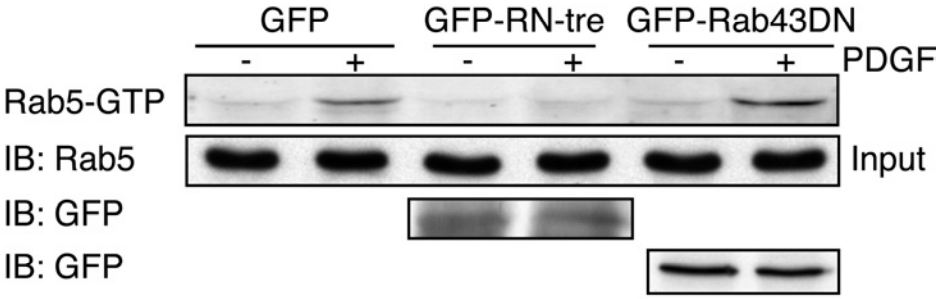
GFP
GFP-RN-tre
GFP-Rab43DN
- + - + - +
PDGF
Rab5-GTP
IB: Rab5
Input
IB: GFP
IB: GFP

O

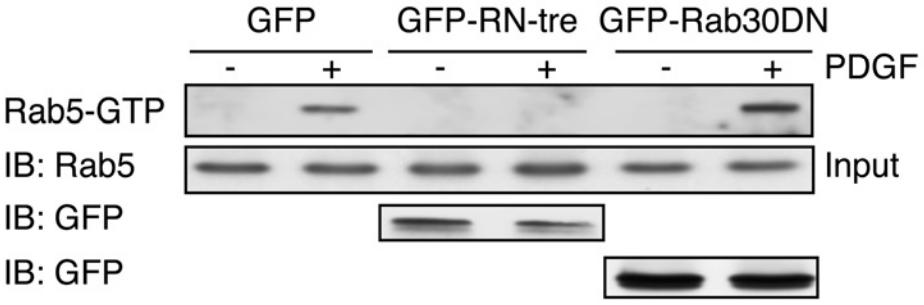
GFP
GFP-RN-tre
GFP-Rab30DN
- + - + - +
PDGF
Rab5-GTP
IB: Rab5
Input
IB: GFP
IB: GFP

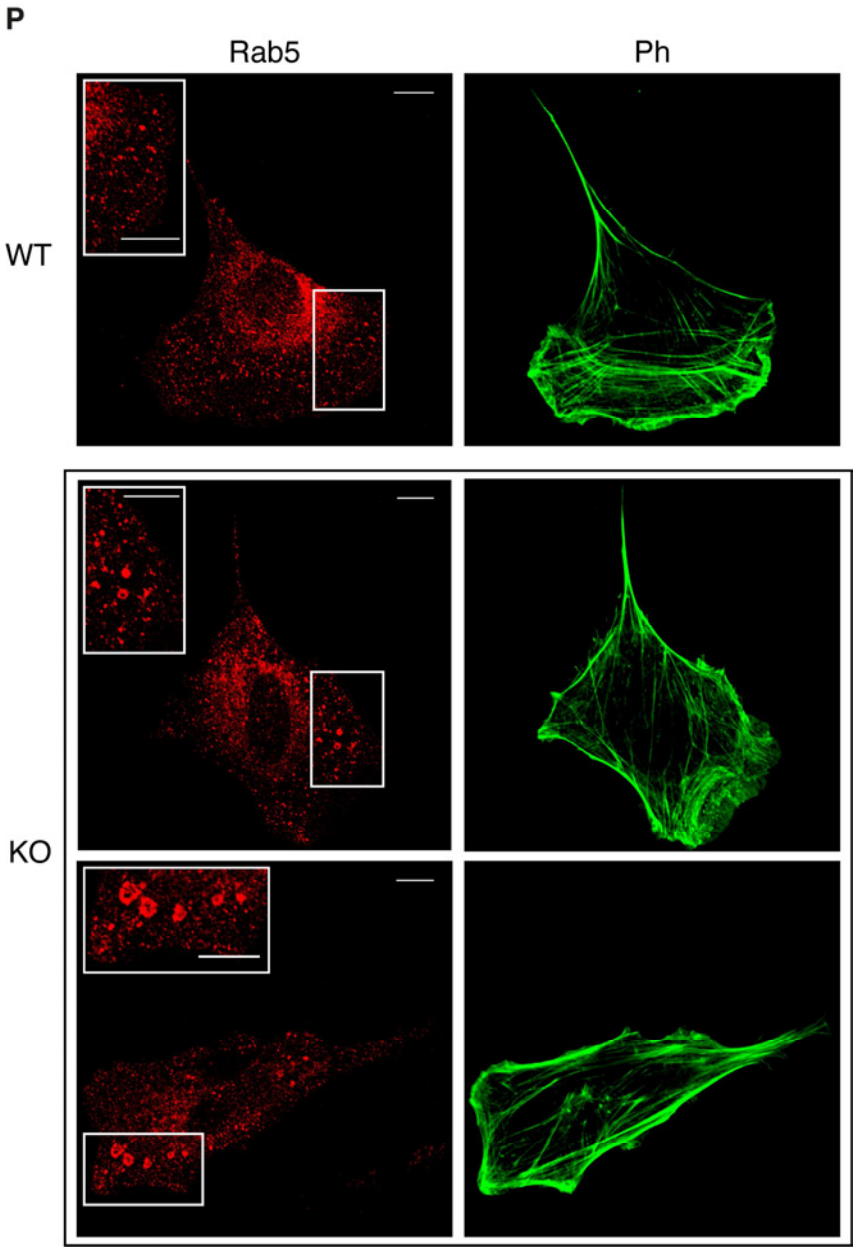

Figure S2, related to Figure 2. GAP assays and generation of *RN-tre* null mice and fibroblasts.

(A) Absence of inorganic phosphate in control GAP preparations or catalytically inactive RN-tre GAP domain. *Left*, Recombinant bacterially-produced GTP-loaded Rab5 (Rab5 alone) used as positive control, or RabGAP-5 and RN-tre TBC domains used at the same

concentration employed in the GAP assays of Figure 2A,C or BSA were analysed using a continuous enzyme-coupled optical assay for the detection of inorganic phosphate with the use of reagents from the EnzChek Phosphate Assay Kit. *Right*, time courses of GTP hydrolysis of 20 μM of Rab5 in the absence (Rab5 alone) or presence of the indicated concentrations of wild type (RN-tre-TBC) or the catalytically inactive RN-tre-TBC^{R150A} (RN-treR150-TBC) domains. (B) TLC-based GAP assays. Recombinant, [γ-^{32}P]GTP-loaded GST-Rab5 (5 μM) was incubated with the indicated concentrations of the TBC domains of either RabGAP-5 or RN-tre. At various time points, Rab5-associated nucleotides were separated by Thin Layer Chromatography (Merck Biosciences), and quantified with a Typhoon Trio. Representative autoradiography is shown on the top. Data are expressed as the % of radioactive GTP over total nucleotide (GTP + GDP) and are the mean ± s.e.m of three independent experiments run in triplicates. Coomassie blue-stained SDS-PAGE of purified TBC domains or of GST-Rab5 are shown on the right or the bottom of the autoradiography, respectively. (C) Representative filter binding GAP assay out of three experiments. Recombinant, [γ-^{32}P]GTP-loaded Rab5 (20 μM) was subjected to filter-binding GAP assays in the presence of 2 μM of control GST (empty circles), GST- RN-tre-TBC (filled circles), or GST-RabGAP-5-TBC (filled squares). After the indicated times, aliquots of the reaction were spotted onto nitrocellulose filters, followed by scintillation counting. GAP activity is expressed as the percentage of non-hydrolysed [γ-^{32}P]GTP that remained bound to the filters, relative to the radioactivity at time 0. Values are the mean ± SD. (D) Baculovirus produced, histidine-tagged full length RN-tre or RabGAP-5 were affinity purified on Nickel-beads and eluted with various concentrations of imidazole as indicated. Purified proteins were resolved by SDS-PAGE and quantified with respect known amounts of BSA. Arrows point at fractions employed in the assays. (E) Targeting strategy. The upper panel depicts the RN-tre genomic locus; shown are the location of the homology arms used for the targeting vector, the

positions of the BamHI sites and the 3' probe (in green) used for Southern blot analysis. The middle panel depicts the targeted locus. The critical Arginine residues in exon 7 and 8 are evidenced in red, also shown are the loxP sides, and the frt sides, contained in the targeting vector, which allow removal of the neo-cassette (indicated as a red box) for the generation of a conditional knockout. The lower panel depicts the locus after deletion of exon 7 and 8 through the action of the Cre-recombinase. In the top and middle panel the BamHI fragments generated in the WT and in the recombinant locus are also indicated in green. (F) Southern blot analysis to detect germline transmission of the targeted allele. Tail DNA from chimeric offspring was digested with BamHI and hybridised with the 3' probe. Digestion with BamHI gives rise to 12.1 and 4.8 kb fragments for the wild type and knockout allele, respectively. The right panel depicts the Southern blot analysis of 2 heterozygous and 2 wild type mice; arrows indicate the expected bands at 12.1 and 4.8 kbp. The left panel shows the Ethidium bromide staining of the gel before transfer. (G) Quantitative RT-PCR analysis of *RN-tre* mRNA in fibroblasts from WT or KO mice. Actin mRNA levels were used as a normalizer. As evident, there is essentially no specific mRNA transcript in KO fibroblasts (the amplified fragment is on exon 3, which is retained in the KO locus), indicating that, as a result of the genetic manipulations, either the *RN-tre* locus underwent major chromatin modifications, resulting in lack of transcription, or that the transcript from the KO locus is unstable. In either case, the results show that *RN-tre* KO mice and fibroblasts are *bona fide* null. (H) Genotyping of embryos. Genotyping was performed by PCR, using a common 5'primer (TF1) and two different a 3'-primers that allowed amplification of either the wild type allele (TF1xTWR2, 550bp) or the knockout allele (TF1xTKR2, 360bp). (I) Ethidium bromide stained gel of a typical PCR reaction. Arrows indicate the amplification products (H, heterozygous mice; WT, wild-type mice; KO, KO mice). (L) Equal amounts of total cellular lysates from WT and *RN-tre* KO primary embryo fibroblasts were immunoblotted with the indicated antibodies.

(M) Equal amounts of total cell lysates from WT, KO, KO+RN-tre and KO+RN-treR150A MEF immunoblotted with the indicated antibodies. Expression of RN-tre or RN-treR150A to levels comparable to endogenous RN-tre was achieved by treating cell populations with 0.5 μg/ml doxycycline for 48 h. (N-O) *RN-tre* KO MEF were transfected with CFP-Rab5 and with GFP (KO), or GFP-RN-tre (RN-tre) or the dominant-negative mutant of GFP-Rab43 (Rab43DN) (N) or the dominant-negative mutant of GFP-Rab30 (Rab30DN) (O). Cells were stimulated with PDGF for 7 min. Input lysates were subjected to GST-EEA1 assay and IB, as indicated. (P) Confocal images of WT and KO MEF (indicated on the left) stained with anti-Rab5 antibody (D-11 Santa Cruz, in red) and phalloidin (green). A portion of each cell has been boxed and magnified in the inset. Two examples of KO fibroblasts are provided. The cell in the bottom panel shows enlarged Rab5-endosomes and it is representative of 30% of total cells in the sample (100 cells/genotype were counted in three independent experiments). Bar, 10 μm.

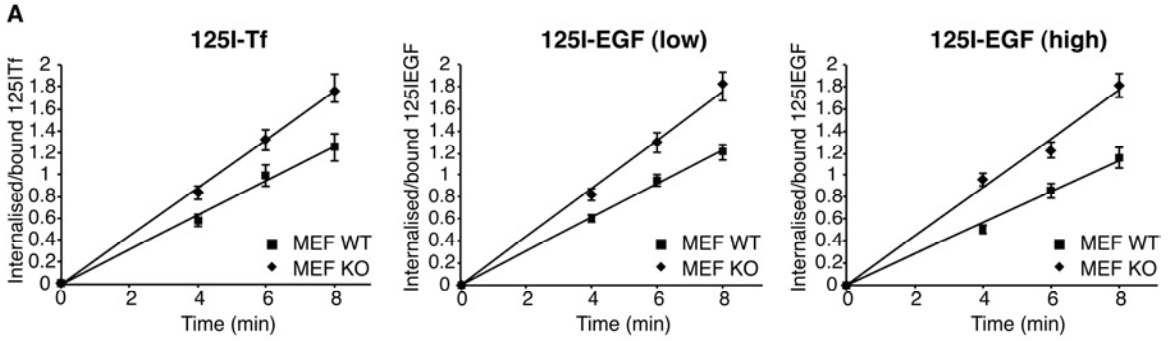

B

Cells	TfRs/cell ($x10^3$)	EGFRs/cell ($x10^3$)	Ke Tf (min^{-1})	Ke EGF Low (min^{-1})	Ke EGF High (min^{-1})
MEF WT	145 ± 7	50 ± 8	0.16 ± 0.013	0.16 ± 0.007	0.16 ± 0.009
MEF KO	110 ± 9	47 ± 5	0.22 ± 0.016	0.21 ± 0.004	0.21 ± 0.01

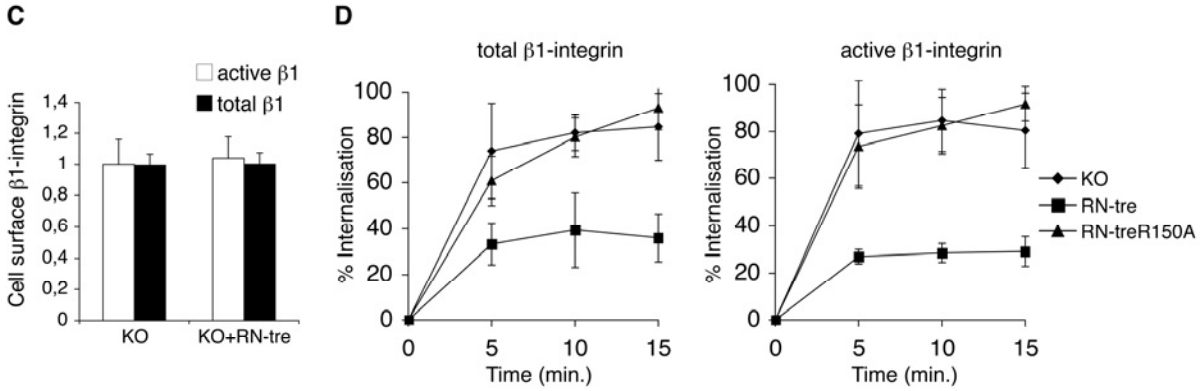

Figure S3, related to Figure 3. Effects of RN-tre on EGFR, TfR and β1-integrin internalisation.

(A) Internalisation kinetics of ^{125}I-Tf (1 μg/ml left panel), ^{125}I-EGF at low dose (1 ng/ml, middle panel) and high dose (20 ng/ml, right panel) (n = 3, mean values ± SD; $p < 0.001$). (B) Summary table of the characterization of *RN-tre* KO and WT MEF. The endocytic rate constant (Ke, min^{-1}) was determined based on the slope of the internalisation kinetics. The number of TfRs and EGFRs at the cell surface was measured by saturation binding assays, as described in Supplemental Experimental Procedures. Mean and standard deviation were

calculated on three independent experiments. Note that MEF KO cells display a lower number of TfRs at the cell surface compared to WT cells, which correlates with their enhanced internalisation. Indeed, TfR is internalised through constitutive endocytosis and therefore the basal number of receptor at the cell surface is sensitive to variations in the internalisation rate. On the contrary, EGFR internalisation is primarily ligand-induced and therefore changes in the EGF-induced internalisation rate do not impact on basal receptor level. *RN-tre* KO and WT MEF display the same receptor number despite the difference in EGFR Ke. (C) Bar graph showing the amount of total (black bars) and active (white bars) β1-integrin at the plasma membrane in *RN-tre* KO MEF expressing empty vector (KO) or RN-tre (KO+RN-tre) measured by ELISA assays (n = 3 mean values ± SD). (D) *RN-tre* KO MEF expressing the inducible empty vector (KO), or RN-tre (KO+RN-tre) or RN-tre^{R150A} (KO+RN-treR150A) were surface labeled with cleavable biotin. Integrin internalization was allowed to for the times indicated, and biotin present on the cell surface was cleaved. The amount of biotinylated intracellular total (graph on the left) or active (graph on the right) β1-integrin was determined with ELISA. The data are expressed as the percentage of internalised receptor relative to the total amount of cell surface–labeled integrin (n = 3, mean ± SD; Mann Whitney test $p < 0.05$).

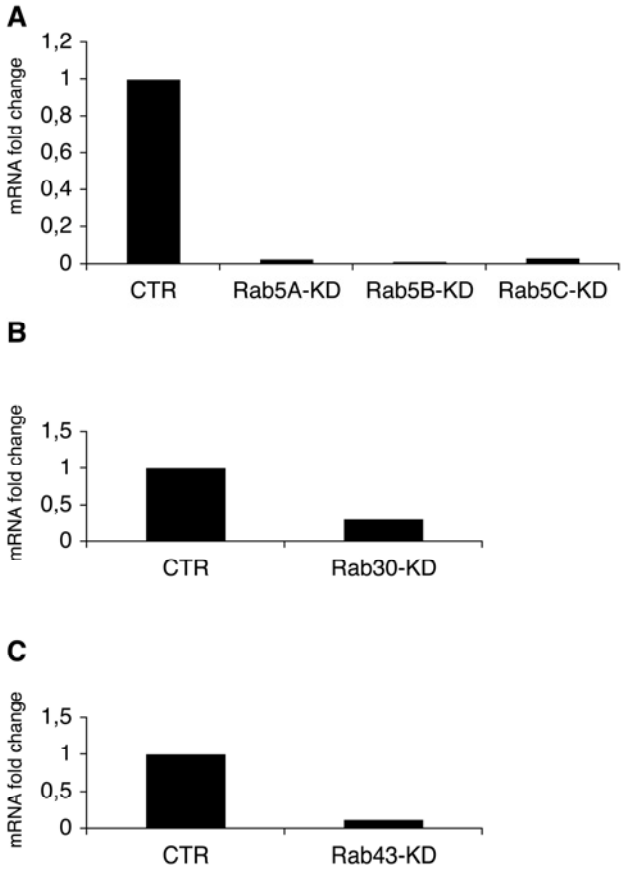

Figure S4, related to Figure 4.

(A-C) KO MEF were transiently transfected with control siRNA oligos (CTR) or oligos for Rab5A/B and C (bar graph in A) or Rab30 (bar graph in B) or Rab43 (bar graph in C) and analyzed for mRNA content by quantitative RT-PCR. mRNA content is expressed as fold change with respect to control RNAi-transfected cells.

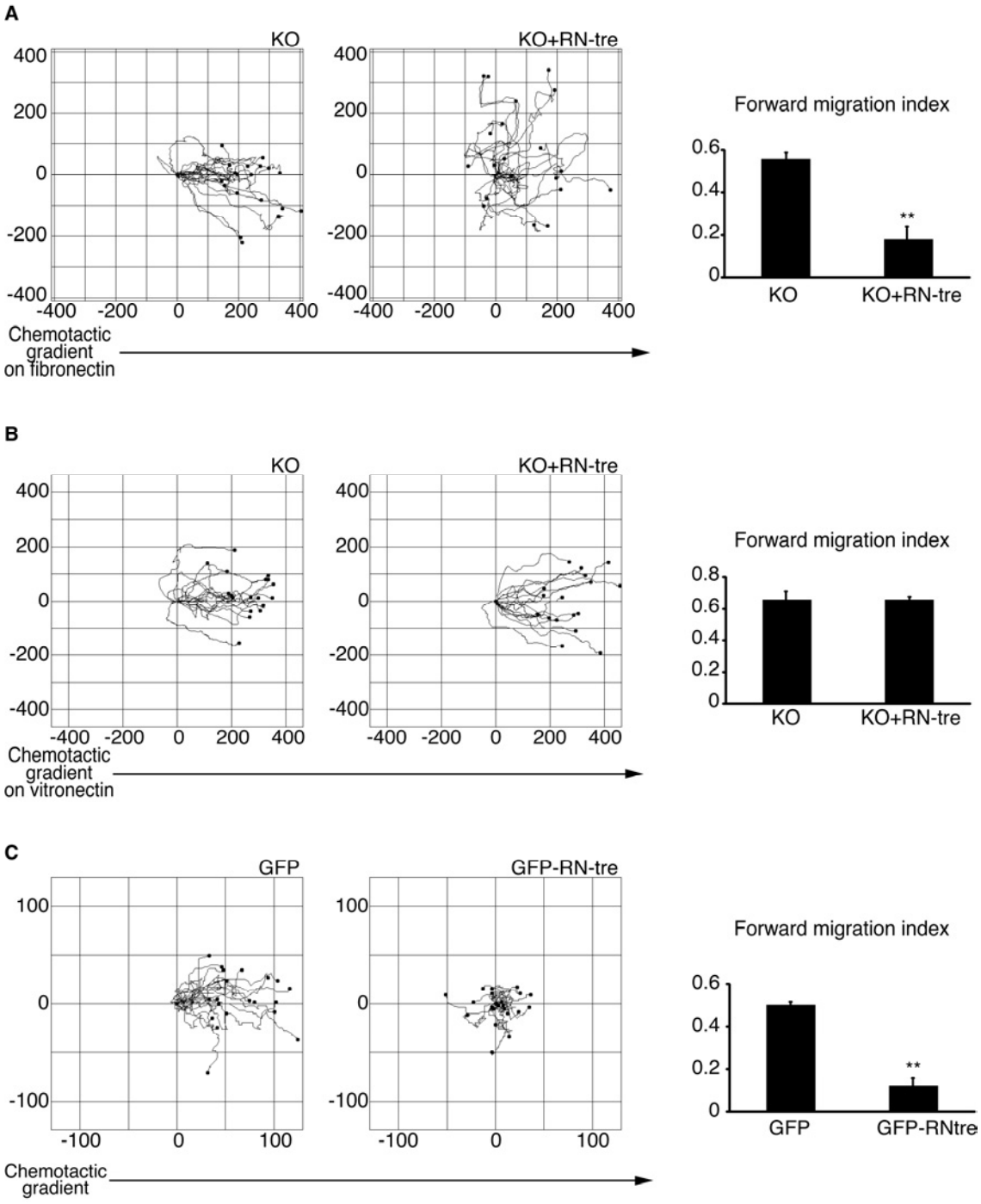

Figure S5, related to Figure 5. RN-tre in cell migration.

(A-B) RN-tre KO MEF expressing or not inducible RN-tre were plated on Dunn chamber pre-coated with either 5 μg/ml of fibronectin (A) or vitronectin (B) and analyzed for chemotactic migration toward a diffusible PDGF gradient. The migratory tracks of some

representative KO or KO+RN-tre MEF were determined as described above. The forward migration index parameter of at least 45 single cells/experiment/condition is plotted in the graphs on the right; **$p < 0.005$. (C) HeLa cells were transfected with GFP-RN-tre or GFP as control. Cell were FACS sorted to isolate GFP-expressing cells and tested in Dunn chamber assays in the presence of a diffusible chemotactic gradient of EGF. Cell migration was tracked every 5 minutes interval over 16 hours period. The migratory tracks of some representative GFP- and GFP-RN-tre expressing HeLa cells are shown. The forward migration index obtained by monitoring at least 50 single cells/experiment/condition is plotted in the graph on the right; **$p < 0.005$.

Legends to Supplemental Movies

Movie S1. TIRF analysis of GFP-RN-tre, RFP-Rab5 and CFP-paxillin. Related to Figure 3.

TIRF imaging of *RN-tre* KO MEF expressing GFP-RN-tre (green) RFP-Rab5A (red) and CFP-paxillin (blue). Co-localisation between Rab5 and RN-tre can be detected on a pool of vesicles in close proximity to remodelling adhesions. Time is in seconds. Bar, 10 μm. Playback is 5 frames/sec.

Movie S2. FRAP analysis of GFP-paxillin turnover in peripheral FA in WT and KO MEF. Related to Figure 4.

Time lapse movie from FRAP of a single GFP-paxillin-positive FA in *RN-tre* WT and KO MEF. Time is in seconds, relative to the time of photobleaching T=0. Bar, 3 μm. Playback is 5 frames/sec.

Movie S3. FRAP analysis of GFP-paxillin turnover in adhesions at the cell rear in WT and KO MEF. Related to Figure 4.

Time lapse movie from FRAP of GFP-paxillin-positive adhesions at the cell rear in *RN-tre* WT and KO MEF. Time is in seconds, relative to the time of photobleaching T=0. Bar, 3 μm. Playback is 5 frames/sec.

Movie S4. FRAP analysis of GFP-paxillin turnover in fibrillar adhesions in WT and KO MEF. Related to Figure 4.

Time lapse movie from FRAP of GFP-paxillin-positive fibrillar adhesions in *RN-tre* WT and KO MEF. Time is in seconds, relative to the time of photobleaching T=0. Bar, 3 μm. Playback is 5 frames/sec.

Movie S5. FRAP analysis of GFP-paxillin turnover in *RN-tre* KO MEF re-expressing RN-tre or its GAP-defective mutant. Related to Figure 4.

RN-tre KO MEF stably transfected with inducible empty vector (KO) or RN-tre (KO+RN-tre) or RN-tre^{R150A} (KO+RN-treR150A) were treated with doxycycline for 48 h to induce the expression of the various proteins. 24 h after induction, cells were transfected with GFP-paxillin and, 24 hours later, subjected to FRAP analysis. Time lapse movie from FRAP of a single GFP-paxillin positive FA in the various cell populations. Time is in seconds, relative to the time of photobleaching T=0. Bar, 3 μm. Playback is 5 frames/sec.

Movie S6. FRAP analysis of GFP-paxillin in Rab-silenced *RN-tre* KO MEF. Related to Figure 4.

RN-tre KO MEF were silenced with control oligos (CTR) or with oligos for Rab5 (Rab5-KD) or for Rab43 (Rab43-KD), transfected with GFP-paxillin and subjected to FRAP analysis. Time lapse movie from FRAP of a single FA in each condition. Time is in seconds, relative to the time of photobleaching T=0. Bar, 3 μm. Playback is 5 frames/sec.

Movie S7. Random motility assay on *RN-tre* WT and KO PEF. Related to Figure 5.

RN-tre WT and KO PEF were plated sparsely, and their motility was monitored by time-lapse video microscopy. Time is in minutes. Bar, 100 μm. Playback is 10 frames/sec.

Movie S8. Chemotaxis assay of *RN-tre* KO inducible MEF. Related to Figure 5.

RN-tre KO MEF stably transfected with inducible empty vector (KO), or RN-tre (KO+RN-tre) or RN-tre^{R150A} (KO+RN-treR150A) were treated with doxycycline for 48 h to induce the expression of the various proteins. 24 h after induction, cells were plated on coverslip,

positioned on a Dunn chamber and monitored by time-lapse microscopy in presence of PDGF gradient. Time is in minutes. Bar, 100 μm. Playback is 10 frames/sec.

Movie S9. Chemotaxis assay of *RN-tre* KO MEF plated on fibronectin. Related to Figure 5.

RN-tre KO MEF stably transfected with inducible empty vector (KO), or RN-tre (KO+RN-tre) were treated with doxycycline for 48 h to induce RN-tre expression. 24 h after induction, cells were plated on coverslip coated with 5 μg/ml fibronectin, positioned on a Dunn chamber and monitored by time-lapse microscopy in presence of PDGF gradient. Time is in minutes. Bar, 100 μm. Playback is 20 frames/sec.

Movie S10. Chemotaxis assay of *RN-tre* KO MEF plated on vitronectin. Related to Figure 5.

RN-tre KO MEF stably transfected with inducible empty vector (KO), or RN-tre (KO+RN-tre) were treated with doxycycline for 48 h to induce RN-tre expression. 24 h after induction, cells were plated on coverslip coated with 5 μg/ml vitronectin, positioned on a Dunn chamber and monitored by time-lapse microscopy in presence of PDGF gradient. Time is in minutes. Bar, 100 μm. Playback is 20 frames/sec.

Movie S11. Chemotaxis assay of HeLa cells overexpressing GFP-RN-tre. Related to Figure 5.

HeLa cells transfected with GFP empty vector or GFP-RN-tre were plated on coverslip, positioned on a Dunn chamber and monitored by time-lapse microscopy in presence of EGF gradient. Time is in minutes. Bar, 50 μm. Playback is 20 frames/sec.

Movie S12. Chemotaxis assay on *RN-tre* KO MEF subjected to siRNA for Rab5, Rab30 and Rab43. Related to Figure 5.

RN-tre KO MEF transfected with control (CTR), Rab5 (Rab5-KD), Rab30 (Rab30-KD) or Rab43 (Rab43-KD) siRNA oligos were plated on coverslip, positioned on a Dunn chamber and monitored by time-lapse microscopy in presence of PDGF gradient. Time is in minutes. Bar, 100 μm. Playback is 10 frames/sec.

Supplemental Experimental Procedures

Expression vectors and antibodies

The identifiers for genes used in the study are: RN-tre, GeneID 9712, Acc. Num. NM_001080491; Rab5A GeneID, 5868, Acc. Num. NM_004162; Rab43, GeneID 339122, Acc. Num. NM_198490; RabGAP-5; GeneID 27352 Acc. Num NM_015705; Rab30, GeneID 27314, Acc. Num NM_014488.

Constructs: GFP-RN-tre and its GAP-defective mutant RN-tre^{R150A} were described in [1], Cherry-RN-tre was subcloned from GFP-RN-tre into pAC Cherry C1 (Clontech), pTagRFP-vinculin was from Evrogen, GFP-paxillin was from Rick Horwitz, GST-TBC domains of RN-tre and RabGAP-5 and his-tagged full length RN-tre and RabGAP-5 were obtained by PCR and cloned respectively in pGEX or in pFastBacHTA vectors. For reconstitution of KO MEF, RN-tre and RN-tre^{R150A} were subcloned from their corresponding pCDNAHA plasmids in the lentiviral TET ON vector pSLIK [2], pGEX-Rab5A and pGEX-EEA1 RBD domain (aa 1257-1411), pCDNA3–Rab5S34N-Myc and pCDNA3–Rab5Q79L-Myc were from Marino Zerial, mRFP-Rab5A was from Addgene, pECFP-Rab5A was from Alexander Sorkin, GFP-tagged dominant-negative point mutants Rab30T23N and Rab43T32N were generated by recombinant PCR and cloned in pEGFPC vectors (Clontech). All constructs used were sequence verified and cloning details are available upon request.

Antibodies were: purified rabbit polyclonal anti-RN-tre (raised against the C-terminal peptide of human RN-tre aa: CLPEVSVDSPVRYKMS and affinity-purified), anti-Rab5 (S-19 and D-11, Santa Cruz), purified rat anti-mouse CD29 (9EG7, BD Pharmingen), mouse monoclonal anti-β1-integrin (JB1B, Abcam ab30388), mouse monoclonal anti-vinculin (clone hVIN-1, Sigma), rabbit monoclonal anti-paxillin (clone Y113, Millipore), rabbit polyclonal anti-β-tubulin (H-235, Santa Cruz), actin was detected with Alexa Fluor 647 Phalloidin (Invitrogen).

RNAi silencing procedures

In the RNAi experiments siRNA oligo duplexes from Invitrogen were transfected with Oligofectamine (according to manufacturer's instructions) and harvested 48 h after transfection.

Sequences of siRNA oligos:

Rab5A: GCAACAAGACCCAACGGGCCAAATA;

Rab5B: CAGGCTGCAATCGTGGTCTATGATA;

Rab5C: CAGATACATTTGCACGGGCTAAGAA.

Rab30: TCCTGAGTGGTTGCGGGAGATAGAA

Rab43: CCAGAGTGGCCACGGAGCTCATCAT

For all siRNA experiments, the appropriate scrambled oligos were used as control siRNAs.

GAP assays

GAP assays using a continuous enzyme-coupled optical assay for the release of inorganic phosphate with the use of reagents from the EnzChek Phosphate Assay Kit (Invitrogen, Carlsbad, CA, USA) were as described in [3]. Data were analysed by fitting them simultaneously to the pseudo-first-order Michaelis–Menten model function $A(t)=(A_\infty-A_0)(1-\exp(-k_{obs}t))+A_0$ where $k_{obs} = k_{intr} + (k_{cat}/K_m)[GAP]$ using GraphPad Prism program. The catalytic efficiency (k_{cat}/K_m) and intrinsic rate constant for GTP hydrolysis (k_{intr}) were treated as global parameters.

TLC-based GAP assays were performed as follows: 500 pmol of purified GST-Rab5 protein bound to glutathione sepharose beads were incubated for 15 min at 30°C with 1.5 pmol of [γ^{32}P]GTP (Perkin Elmer) and 800 pmol of cold GTP (Sigma-Aldrich) in 40 mM Tris–HCl (pH 7.5), 50 mM NaCl, 5 mM EDTA, 1.74 mM $MgCl_2$, 0.5 mM DTT, 0.36%(w/v) CHAPS,

and 1 mg/mL BSA. The loading reaction was stopped by washing the resin with ice-cold wash buffer containing 20 mM Tris–HCl (pH 8.0), 100 mM NaCl, 20 mM $MgCl_2$, and 0.5 mM DTT. The GTPase activity reaction was initiated by adding GST-TBC protein (50 or 150 pmol for RabGAP-5 and RN-tre), and incubated at 30°C for 5 or 10 min. After extensive washing of the resins with ice-cold wash buffer, associated nucleotides were separated by Thin-Layer Chromatography (Merck Biosciences), and quantified with a Typhoon Trio (GE healthcare), as described [4]. Filter binding GAP assays were as described in [1].

Pull down assays for detection of Rab5-GTP

Pull-down assays of Rab5-GTP were performed with GST-EEA1$^{1257\text{-}1411}$ (GST-EAA1) purified from *E. coli* BL21 (DE) bacterial cells, as described in [5]. *RN-tre* WT or KO fibroblasts were lysed with Pull-Down Lysis Buffer [50 mM Tris HCl pH 7.4, 150 mM NaCl, 1% NP-40, 5% glycerol, 1 mM EDTA, 10 mM $MgCl_2$, proteases inhibitor cocktail (Calbiochem)]. Lysates (3-5 mg) were incubated with 30 μg of purified GST-EEA1 conjugated to glutathione-Sepharose beads, for 1 h at 4°C. Beads were washed with Pull-Down Lysis Buffer three times at 4°C. Specifically-bound material was analysed by SDS-PAGE and immunoblot as described [6].

Transferrin and EGF internalisation assays

Internalisations of ^{125}I-EGF and ^{125}I-Tf (purchased from Perkin Elmer) were performed as described [7, 8]. Briefly, cells were serum starved for 2-4 hours and then incubated at 37°C in the presence of ^{125}I-EGF and ^{125}I-Tf at the indicated concentration in binding medium (BSA 0.1%, 20 mM Hepes pH 7.4). After the indicated time points, cells were washed three times in PBS, and then surface-bound radioactivity was removed through an acid wash pH 2.5 (acetic acid 0.2 M, NaCl 0.5 M) and measured. This sample represents the amount of ^{125}I-

EGF and ^{125}I-Tf bound to the receptors on the cell surface. Cells were then lysed in 1M NaOH. This sample represents internalized ^{125}I-EGF and ^{125}I-Tf. The unspecific binding was measured at each time point in the presence of 300-fold excess of non-radioactive EGF/Tf. After being corrected for non-specific binding, the rate of internalisation was expressed as the ratio between internalised and surface-bound radioactivity. From the kinetics, we calculated the endocytic rate constant (Ke).

Saturation binding assay

Surface EGFRs were measured by ^{125}I-EGF saturation binding [8]. Briefly, cells were serum starved for 2-4 hours and then incubated on ice in the presence of 100 ng/ml EGF (5 ng/ml ^{125}I-EGF + 95 ng/ml cold EGF) or 2 μg/ml Tf, in binding medium (BSA 0.1%, 20 mM Hepes pH 7.4). After six hours, cells were washed three times in PBS, and then were lysed in 1M NaOH. The unspecific binding was measured in presence of an excess of 300-fold non-radioactive EGF.

SUPPLEMENTAL REFERENCES

1. Lanzetti, L., Rybin, V., Malabarba, M.G., Christoforidis, S., Scita, G., Zerial, M., and Di Fiore, P.P. (2000). The Eps8 protein coordinates EGF receptor signalling through Rac and trafficking through Rab5. Nature *408*, 374-377.
2. Shin, K.J., Wall, E.A., Zavzavadjian, J.R., Santat, L.A., Liu, J., Hwang, J.I., Rebres, R., Roach, T., Seaman, W., Simon, M.I., et al. (2006). A single lentiviral vector platform for microRNA-based conditional RNA interference and coordinated transgene expression. Proc Natl Acad Sci U S A *103*, 13759-13764.
3. Pan, X., Eathiraj, S., Munson, M., and Lambright, D.G. (2006). TBC-domain GAPs for Rab GTPases accelerate GTP hydrolysis by a dual-finger mechanism. Nature *442*, 303-306.
4. Kajiho, H., Sakurai, K., Minoda, T., Yoshikawa, M., Nakagawa, S., Fukushima, S., Kontani, K., and Katada, T. (2011). Characterization of RIN3 as a guanine nucleotide exchange factor for the Rab5 subfamily GTPase Rab31. J Biol Chem *286*, 24364-24373.
5. Simonsen, A., Lippe, R., Christoforidis, S., Gaullier, J.M., Brech, A., Callaghan, J., Toh, B.H., Murphy, C., Zerial, M., and Stenmark, H. (1998). EEA1 links PI(3)K function to Rab5 regulation of endosome fusion. Nature *394*, 494-498.
6. Fazioli, F., Minichiello, L., Matoska, V., Castagnino, P., Miki, T., Wong, W.T., and Di Fiore, P.P. (1993). Eps8, a substrate for the epidermal growth factor receptor kinase, enhances EGF-dependent mitogenic signals. Embo J *12*, 3799-3808.
7. Haglund, K., Sigismund, S., Polo, S., Szymkiewicz, I., Di Fiore, P.P., and Dikic, I. (2003). Multiple monoubiquitination of RTKs is sufficient for their endocytosis and degradation. Nat Cell Biol *5*, 461-466.
8. Tosoni, D., Puri, C., Confalonieri, S., Salcini, A.E., De Camilli, P., Tacchetti, C., and Di Fiore, P.P. (2005). TTP specifically regulates the internalization of the transferrin receptor. Cell *123*, 875-888.